Ph. D. Thesis
박사 학위논문

Soft Computing Approach for Sensorless Control in Brake-By-Wire Systems with Electro-Mechanical Brake

Junhyung Bae(배 준 형 裵 浚 亨)

Department of
Information and Communication Engineering
정보통신융합공학전공

DGIST

2017

Ph. D. Thesis
박사 학위논문

Soft Computing Approach for Sensorless Control in Brake-By-Wire Systems with Electro-Mechanical Brake

Junhyung Bae(배 준 형 裵 浚 亨)

Department of
Information and Communication Engineering
정보통신융합공학전공

DGIST

2017

Soft Computing Approach for Sensorless Control in Brake-By-Wire Systems with Electro-Mechanical Brake

Advisor : Professor Yongsoon Eun

Co-advisor : Professor Jong-Hae Kim

by

Junhyung Bae
Department of Information and Communication Engineering
DGIST

A thesis submitted to the faculty of DGIST in partial fulfillment of the requirements for the degree of Doctor of Philosophy in the Department of Information and Communication Engineering. The study was conducted in accordance with Code of Research Ethics[1].

5. 26. 2017

Approved by

Professor Yongsoon Eun _____
(Advisor)

Professor Jong-Hae Kim _____
(Co-Advisor)

[1] Declaration of Ethical Conduct in Research**:** I, as a graduate student of DGIST, hereby declare that I have not committed any acts that may damage the credibility of my research. These include, but are not limited to: falsification, thesis written by someone else, distortion of research findings or plagiarism. I affirm that my thesis contains honest conclusions based on my own careful research under the guidance of my thesis advisor.

Soft Computing Approach for Sensorless Control in Brake-By-Wire Systems with Electro-Mechanical Brake

Junhyung Bae

Accepted in partial fulfillment of the requirements for
the degree of Doctor of Philosophy

5. 26. 2017

Head of Committee _____(인)
Prof. Minkyu Je

Committee Member _____(인)
Prof. Jong-Hae Kim

Committee Member _____(인)
Prof. Yongsoon Eun

Committee Member _____(인)
Prof. Kyung-Joon Park

Committee Member _____(인)
Dr. Seonghun Lee

Ph. D/IC
201232002

배 준 형. Junhyung Bae. Soft Computing Approach for Sensorless Control in Brake-By-Wire Systems with Electro-Mechanical Brake. Department of Information and Communication Engineering. 2017. 114p. Advisors Prof. Yongsoon Eun, Prof. Co-Advisors Jong-Hae Kim.

ABSTRACT

In this thesis, we propose a new soft computing-based approach for sensorless fault-tolerant control in brake-by-wire (BBW) systems.

Research on BBW systems in the automobile industry is actively proceeding. In order to mount and drive the electro-mechanical brake (EMB) used as the brake actuator in the hybrid vehicles and electric vehicles for operation reliability it is imperative that the clamping force data is not lost even if a failure occurs in the electrical and electronic systems.

In this study, the mathematical modeling of the mechanical part and the electric motor of the EMB system was first established and the cascaded PI controller was designed based on the EMB model. The mechanical part consisted of a reduction gear, screw, inner/outer pads, and caliper. A permanent magnet synchronous motor (PMSM) was used for the electric motor and an electronic control unit (ECU) including the micro-controller and the inverter was constructed and experiments were performed. The EMB controller is configured as a cascaded PI control type, and the clamping force controller, speed controller, and the current controller are located in the order of the external controller to the internal controller. The gain of the controller is designed to be easily adjusted using the parameters of the motor. Also, the vector control method was applied to the PMSM to ensure optimal torque operation.

Our goal is to apply a new hybrid-type system identification and estimation methods against failure or for sensorless control that can occur in the EMB electronic pedal sensor system and the clamping force sensor by applying the soft computing techniques such as a neural network, fuzzy and genetic algorithm.

First, we propose a novel identification of an electronic brake pedal system for a virtual sensor system based on a hybrid approach using the group method of data handling (GMDH) and the genetic algorithm (GA). The main idea in the GMDH is to build an analytical function in a feed-forward network based on a quadratic node transfer function whose coefficients are obtained using a regression technique. The analytical GMDH model has been found, and application of this model is very quick and inexpensive compared to other identification techniques. To develop the best network architecture for the GMDH, the GA is arranged in a new approach to design the whole architecture of the GMDH.

Second, we study estimation of the clamping force in the EMB actuator part. The main sensors used in the EMB control system are a clamping force sensor to measure clamping force, a rotor position sensor to measure motor rotation angle, and a current sensor to measure the current of the three-phase motor. It is necessary to judge the failure of each sensor or developing without sensors in terms of cost and implementation and replace with an appropriate estimation value in the case of failure. In this study, the estimation of the clamping force is more accurate considering the hysteresis at the time of applying and releasing, and the dynamic stiffness model and torque balance model are combined by using a novel Kalman filter optimized by the GA. The application of the GA improves the estimation accuracy by optimizing the noise covariance matrices of the Kalman filter and enables on-line estimation when using a high performance parallel processor.

Finally, we verified the performance of the proposed algorithm through experiments.

Keywords: Brake-by-wire, Electro-mechanical brake, Group method of data handling, Genetic algorithm, Kalman filter

Contents

List of tables

List of figures

I. Introduction

1.1 Background and Motivation

In future cars, X-by-wire systems will be introduced to implement various advanced functions. The technology to control the target plant by removing the mechanical link or the hydraulic line and transmitting an electric signal shows better performance in terms of space, cost, function, and environment. Since the parts can be modularized, it is possible to apply one designed system to various models without changing the structure, which is advantageous in terms of production cost. This technology is also environmentally friendly because it is relatively lightweight and fast in response and suitable for performing chassis control functions and does not use hydraulic oil [1].

X-by-wire systems can be divided into drive-by-wire (DBW), steer-by-wire (SBW), and brake-by-wire (BBW) depending on the purpose of use. The technique of replacing mechanical connections with the transmission of electrical signals can improve performance with the development of in-vehicle network systems. In order to apply X-by-wire to real vehicles, it is necessary to improve the reliability and to develop a large capacity power system [2].

The BBW systems related to braking via X-by-wire can be classified into hydraulic drive type electro-hydaulic brake (EHB) and electric drive type electro-mechanical brake (EMB) or electro-wedge brake (EWB) depending on the drive type [3]. The EHB has been developed based on hydraulic braking technology using existing mechanical devices. However, by replacing the physical control using mechanical devices with electronic parts and signals, due to the durability and complicated structure of the electronic parts constituting

EHB, EMB and EWB technology is under development. Figure 1.1 shows the technology roadmap for the vehicle braking system [4]. In the case of EHB, Bosch (Germany) produced the sensortronic brake control (SBC) system and Delphi (USA) developed the Galileo system [5]. In particular, the Galileo system is equipped with a front wheel braking system that is a mixture of electric and hydraulic, and mechanical devices such as electric motors and bearings on the rear wheels. The EMB system which has yet to be mass-produced but, is a key part of BBW, is an electro-mechanical braking method that uses an electric motor to brake the vehicle, unlike conventional hydraulic brakes. This system is characterized by a completely dry electrical component system that replaces conventional actuators with electric motor-driven units (see also Figure 1.2). It shows a faster response than existing methods for applying brake control technology such as anti-lock braking system (ABS) or electronic stability control (ESC) [6]. However, the EMB requires large power for braking the front wheels, and it suffers from reduced efficiency due to friction between the screw and gear system, degraded actuator efficiency due to environmental changes such as temperature and humidity, and a communication problem for real-time control. Furthermore, the clamping force sensor is costly. The EWB has been studied to solve the problem of high voltage required to generate high braking force. The EMB is a method to generate braking force by inputting torque generated by an electric motor, but EWB can ensure the same braking force with less power consumption than EMB by using disk rotating force as braking force by using a wedge in the caliper part.

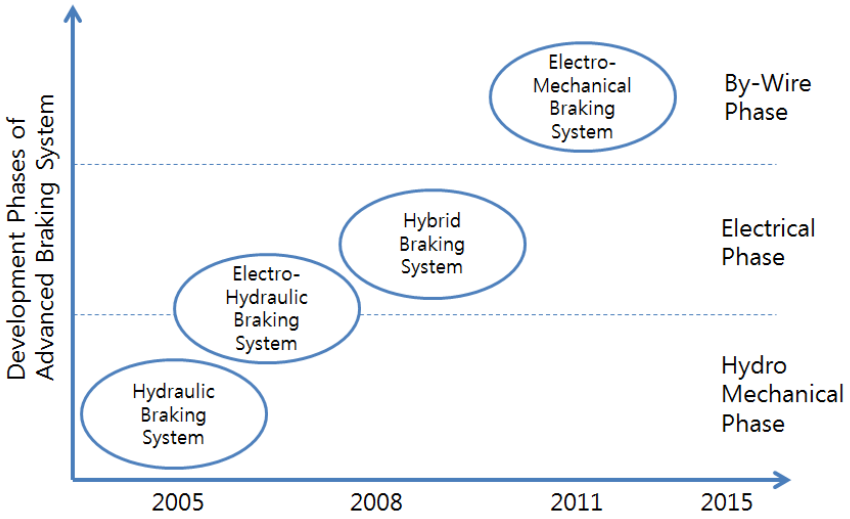

Fig. 1.1. Roadmap for the automotive brake system

Fig. 1.2. Electro-mechanical brake system (developed by DGIST)

The demand for space constraints and light-weight automobiles has led to the adoption of permanent magnet synchronous motors (PMSMs) as actuators in electronic control systems. PMSMs are widely used as actuators in various industrial fields because of their higher energy density and easier maintenance than DC motors or induction motors. As automotive components, PMSM drive systems must operate at low cost and have a long service life corresponding with the life cycle of the vehicle and maintain high system reliabil-

ity.

The control methods of PMSMs used as an actuator in EMBs have been widely studied. Field-oriented control (FOC) or vector control, which controls the torque by controlling the magnitude and phase direction of the stator current based on the flux vector in space, is widely used. A study on clamping force control of the EMB has been carried out [7]. The authors proposed a method to detect the contact point between the pad and the disk by constructing an EMB control system incorporating a current controller, speed controller, and the force controller. Line et al. [8] designed a PI controller to avoid the use of the maximum speed, maximum power, and maximum current of the motor during clamping force control. They developed a simulator including the Coulomb friction model of the motor and the back-EMF model, and evaluated the efficiency of the controller. In order to solve the problem of instability of the PI controller due to the nonlinear characteristics of the EMB actuator, a study using the model predictive control (MPC) method was also performed [9]. In addition, an optimal control method was proposed to efficiently control the EMB while minimizing power consumption in various disturbance input environments [10].

Due to the increase of new electronic sensors, actuators, and electronic control unit (ECU) devices in tandem with strengthened environmental and safety regulations in the automobile industry and demand for consumer convenience, it is necessary to replace conventional mechanical and hydraulic controlled steering or braking devices with electronic control methods and related research is actively under way. Eco-friendly cars such as hybrid and electric vehicles are accelerating this trend [11].

In an EMB system, failure of the PMSM drive and pedal system including ECUs may affect the safety of the entire vehicle and lead to personal injury. Therefore, various fault-tolerance techniques including fault detection are needed. Effective fault-tolerance can increase the reliability of the system and reduce the occurrence of additional maintenance

costs [12-14].

Fault-tolerance can be divided into hardware redundancy and analytic redundancy. The hardware redundancy method has the advantage of using two or more hardware having the same function to allow failure, and is the most reliable and simple method to implement. However, it has the disadvantage of a complicate structure and incurs additional costs. To resolve the drawbacks of hardware redundancy, the concept of analytic redundancy has been studied since the 1970s [15, 16]. Even if a device plays a different role, the same effect as using hardware redundancy can be obtained by using information about the dynamic characteristics inside the system.

In the EMB, it is difficult to mount a torque sensor or a clamping force sensor due to the complicate structure and the additional cost, and studies have been conducted to control the EMB without a clamping force sensor. Since such sensorless control methods are mainly used for EMB control by estimating the clamping force, it is possible to detect faults for fault-tolerance and use them for controller redesign. A method of estimating the clamping force by calculating the average value of the motor torque at the time of increasing and decreasing the clamping force and using the torque-force relationship has been proposed [17]. However, this method produces an error in estimating the clamping force when the motor rotates at a high speed. Saric et al. [18] proposed an estimation method based on the relationship between the rotation angle of the motor and the clamping force. In addition, a technique has been developed to accurately estimate the rotation angle and the speed of a motor using a resolver signal [19]. Most recently, Eum et al. [20] proposed a robust sensorless control method for an EMB system that can be applied to commercial city buses. A cascade control strategy is proposed and a disturbance observer is employed to enhance the control robustness against model variations.

Due to the industrial property rights within the automotive industry, very little stud-

ies have been published. There are no previous studies describing actual tests and performance results of BBW with EMB beside those that have been carried out through the Ref. [21].

1.2 Research Objective and Contribution

This thesis proposes a soft computing-based approach to identification of the electronic brake pedal system of the BBW and to estimate the clamping force which is the core technology the of BBW among the increasingly electronic automobile chassis control technology.

During the last four decades, researchers have proposed many model-based control strategies. In general, these design approaches involve various phases such as modeling, analysis, simulation, implementation, and verification. These conventional model-based methods have been practically applied and have provided satisfactory solutions for the complex systems under various uncertainties. However, as Zadeh articulated as early as 1962, “often the solution of real life problems in system analysis and control has been subordinated to the development of mathematical theories that dealt with over-idealized problems bearing little relation to theory” [22].

In a broad perspective, intelligent systems underlie what is called “soft computing” [23]. In traditional hard computing, the main purposes of the computations are precision and certainty. In soft computing, however, the precision and certainty are costly. Therefore, it is realistic to consider the integration of computation, reasoning and decision making for the trade-off between precision and uncertainty. This integration of methodologies provides a foundation for the conceptual design and deployment of intelligent systems. The theories

are fuzzy logic, neural network, genetic algorithm, and probabilistic reasoning. Furthermore, these methodologies are complementary rather than competitive. Increasingly, these approaches are also utilized in combination, and referred to as “hybrid”. Presently, the most well-known systems of this type are neuro-fuzzy systems. Hybrid intelligent systems are likely to play a critical role for many years to come [24].

Unlike model-based methods, soft computing methodologies mimic consciousness and cognition in several important ways: they can learn from experience; they can universalize into domains where direct experience is absent; and through parallel computer architectures that simulate biological processes, they can quick perform an input-to-output mapping rather than inherently serial analytical representations [25, 26].

An identification approach for linear or non-linear system, which is the basis of the input/output data and regression analysis of the prediction problem, is useful. However, if the system to be modeled is a complex and large-scale structure, the regression analysis cannot be applied because the input/output relationship is not limited to a representable functional type. In general, complex multivariate modeling has the following problems [27].

- Among many input variables, we cannot determine the variables that make up the model.
- The structure of the model (function form) cannot be determined.
- If the number of coefficients to be estimated is large, the amount of data required for estimation becomes large.

In order to solve this problem, a method based on the discrimination by Volterra series or a polynomial expression of Kolmogorov-Gabor has been proposed. Group method of data handling (GMDH) is a valid method for this kind of problem. It is one of the most powerful tools that have been widely employed in recent years in various fields such as

sensors, measurement and control, and engineering [28]. GMDH was proposed by A. G. Ivakhnenko [29], and nonlinear model estimation is obtained by hierarchically combining partial expressions by quadratic expression of two variables in the case of nonlinear relations in which the input/output relation or function type of the model is not specially defined. Regression analysis by partial expression is applied at each hierarchy. By applying the quadratic expression of two variables, nonlinear functions of input/output relations can be easily obtained, and it is possible to identify and predict complex multivariable and nonlinear systems with small data. Over the past 40 years it has been improving and evolving, first by works in the field of what was known in the USA as adaptive learning networks in the 1970s and 1980s and later by significant contributions from scientists from Germany, Ukraine, Japan, and China, etc.

The unique feature of the self-organizing modeling approach of GMDH is that it allows, systematically and autonomously, optimal complex models to be developed by performing both parameter and structure identification. It inductively builds the model structure or composition of terms or network topology, automatically. This is possible, because self-organizing modeling closely links model accuracy to model complexity. It introduces the concept of an optimal complex model as a model that optimally balances model quality on a learning data set and its generalization power on new, not previously seen data with respect to the data's noise level and the purpose of modeling. This has been the key idea for solving the basic problem of experimental systems analysis of avoiding over-fitted models based on the data's information, and this makes advanced implementations of this algorithm a powerful, efficient, and easy-to-use knowledge extraction tool [30].

Today, in engineering, there is a spectrum of self-organizing modeling algorithms. This thesis adds to this spectrum a new element by combining GMDH with other state-of-the-art soft computing methods. The main idea of this work is to develop a mathematical

model to identify the electronic brake pedal system using hybrid soft computing in our BBW systems. Thus, instead of directly using a physical device, we introduce a virtual sensor (or soft sensor) system that includes alternative devices that are easier to implement. The virtual sensor is a valuable tool in many different industrial fields of application. It is expected to solve a number of different problems such as measuring system back-up, real-time prediction for control, and fault diagnosis strategies.

The successful use of a clamping force sensor in the EMB poses a challenging engineering task. In order to implement various chassis control functions in the EMB, it is important to accurately feedback the clamping force of the system. If a clamping force sensor is placed close to a brake pad, it will then be subject to severe high temperature that will challenge its mechanical integrity. This situation can be avoided by embedding a clamping force sensor deep within the EMB, i.e. at the near end of the ball-screw. It has been shown that embedding this sensor leads to hysteresis, which is influenced by friction between the clamping force sensor and the pad and disk interface. This hysteresis significantly influences the accuracy of clamping force measurement. In addition, it is costly to mount a sensor to measure the clamping force. Due to the cost and engineering problems involved with including the clamping force sensor, it is highly desirable to eliminate this component from the BBW systems. A potential opportunity to achieve this lies in the development of a virtual sensor. That is, to accurately estimate the clamping force based on alternative measurements leading to the omission of a clamping force sensor. This thesis further develops a virtual clamping force sensor that can lead to the omission of a physical force sensor in our EMB systems. Therefore, the clamping force can be estimated without a physical sensor by combining the dynamic stiffness model and torque balance model with a hybrid genetic algorithm and Kalman filter. The EMB test bench was developed and the validity was verified through experiments.

1.3 Thesis Organization

This thesis is organized as follows: in chapter 2, mathematical modeling and controller design of an EMB system are performed. Nonlinear characteristics such as friction and backlash were simulated. Chapter 3 describes the identification of the electronic brake pedal system using hybrid GMDH/GA. Experimental results are compared with other traditional methods. In chapter 4, we propose a clamping force estimation method combining two models by a hybrid genetic algorithm and Kalman filter. Finally, we discuss possible future works and conclude this thesis in chapter 5.

II. Modeling and Control of Electro-Mechanical Brake System: Basic Principle

2.1 Introduction

The X-by-wire (XBW) systems have the advantage of improving vehicle design flexibility and fuel economy by replacing existing complex mechanical systems with electrical systems using in-vehicle networks. Among the XBW systems, the brake-by-wire (BBW) systems use sensors and actuators to replace the existing hydraulic system components such as pumps, hoses, oil, vacuum servos, and master cylinders, thus providing the advantages of fast braking and accuracy including the above advantages. The BBW systems use an electro-mechanical brake (EMB) as a wiring harness and a brake actuator instead of the conventional hydraulic and mechanical link [31].

The EMB is an eco-friendly BBW system that does not use hydraulic pressure. It generates braking force using a motor with a fast response. Therefore, the braking force response characteristic is relatively fast. This characteristic enables control of new concepts as well as an anti-lock braking system (ABS), traction control system (TCS), and electronic stability program (ESP) control. However, the EMB requires large power for braking the front wheels, and it has a power problem of the 12 V power system, reduced efficiency due to friction between the screw and gear system, degraded actuator efficiency due to environmental changes such as temperature and humidity, and communication problems for real-time operation, as well as requiring a costly clamping force sensor [32].

The EMB can be divided into a screw-type EMB with screw direct pressurization and an electro-wedge brake (EWB) with wedge. Figure 2.1 shows the screw-type EMB and

the wedge-type EWB structure.

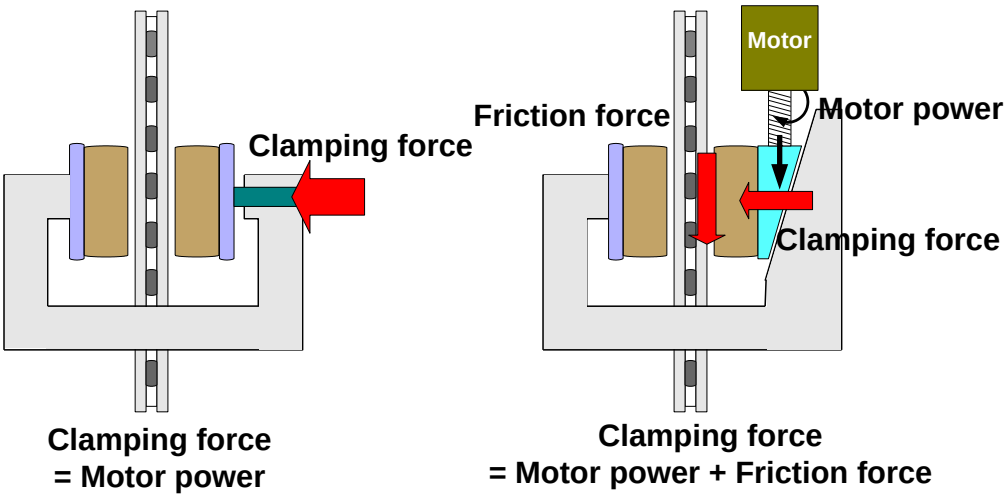

Fig. 2.1. Structures of the EMB and EWB

The screw-type EMB presses the pad onto the disk through the piston connected to the screw. The wedge-type EWB uses self-reinforcing to push the wedge again by the force of the wedge through the screw and the braking frictional force. The EWB has advantages of reducing the driving power of the actuator and increasing the efficiency of the system by self-boosting, but it may incur jamming due to the wedge, which requires more precise high performance control [33, 34]. Currently, the EMB was developed by TRW, Bosch, Hyundai Mobis, Mando, erae Automotive Systems, etc. and the EWB was developed in Siemens VDO but has not yet reached the practical stage [35-38].

Figure 2.2 shows the structure of a typical BBW system. The operation of the BBW system causes the electronic brake pedal according to the braking input, which occurs when the driver depresses the pedal. At this time, the central electronic control unit (ECU) determines the required braking force by using the position signal of the pedal, and determines the target braking force of each wheel through cooperative control with the regenerative braking device. The ECU of each wheel controls the EMB to generate the target braking

force transmitted from the central ECU. The EMB receives the braking command from the actuator ECU and generates the braking force from the electric motor, gear, and screw mechanism. In order to provide regenerative braking coordination control, an electronic brake system with fast a response such as the EMB is indispensable, and high performance control of the motor applied to the EMB is essential to generate this target braking force accurately and quickly.

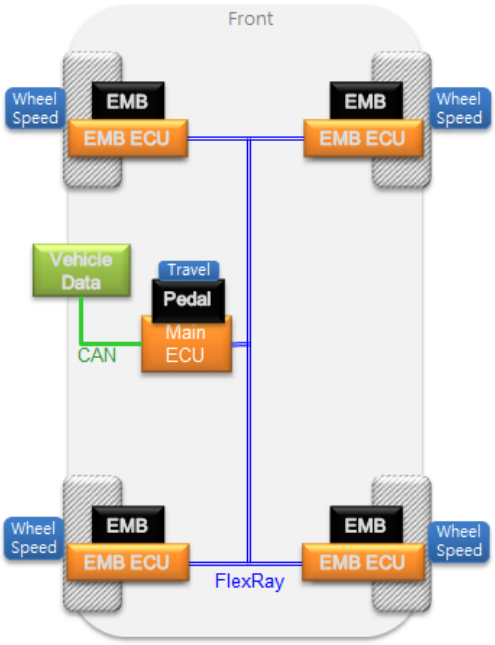

Fig. 2.2. BBW system architecture

In this chapter, mathematical modeling is established for the EMB system applying a permanent magnet synchronous motor (PMSM) as an actuator. The cascade PI controller was then designed. The modeling of the components is based on Ref. [31]. The system models are implemented by MATLAB/Simulink.

2.2 Modeling of the EMB System

The EMB system consists of an electric motor, a planetary gear reducer, a screw gear, an inner/outer pad, and a caliper, as shown in Figure 2.3. The rotational motion of the motor is converted into a linear motion by a screw thread, and a clamping force is generated between the brake pads and the disk by the force.

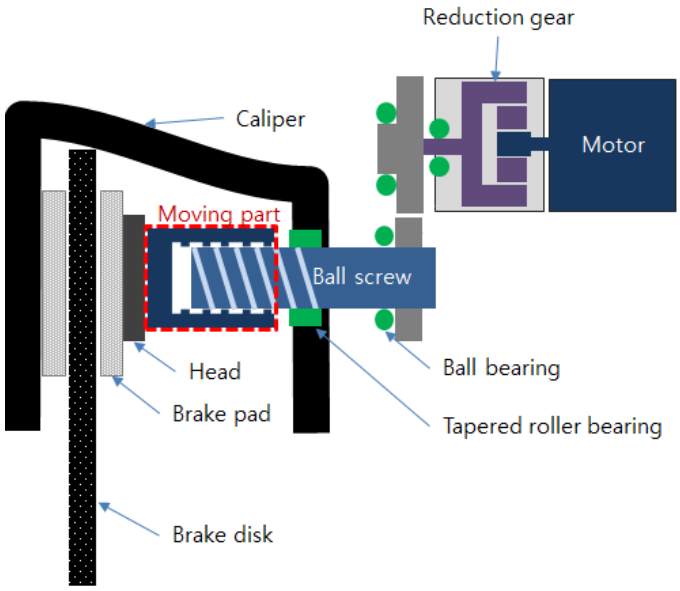

Fig. 2.3. Configuration of the EMB

2.2.1 Modeling of the PMSM

Modeling of the PMSM uses reference frame transformation. Reference coordinate system transformation is a commonly used method for easily modeling, analyzing, and controlling an AC system, and it converts coordinate systems such as voltage, current, and magnetic flux into an easy to use system. The voltage equation of the PMSM used in the EMB system is expressed in the form of a time-varying differential equation when the motor rotates. The three-phase source of a, b, and c phase is converted into a coordinate

system of d-axis, q-axis, and n-axis through reference coordinate system conversion. Here, the d-axis is the axis on which the excitation flux exists in a direct axis. The q-axis is a quadrature axis, and the electrical angle is positioned by a phase difference of 90 degrees ahead of the direct axis in the forward rotation. The n-axis is the neutral axis and does not affect the formation of the rotor [39-41].

Conversion of d, q, and n to the stationary coordinate system in the a, b, and c coordinate system and vice versa can be obtained through the Park's transformation and the inverse transformation of Eqs. (2.1) and (2.2), respectively.

$$\begin{bmatrix} f_q \\ f_d \\ f_n \end{bmatrix} = \frac{2}{3} \begin{bmatrix} \cos\theta_r & \cos\left(\theta_r - \frac{2\pi}{3}\right) & \cos\left(\theta_r + \frac{2\pi}{3}\right) \\ \sin\theta_r & \sin\left(\theta_r - \frac{2\pi}{3}\right) & \sin\left(\theta_r + \frac{2\pi}{3}\right) \\ \frac{1}{2} & \frac{1}{2} & \frac{1}{2} \end{bmatrix} \begin{bmatrix} f_a \\ f_b \\ f_c \end{bmatrix} \tag{2.1}$$

$$\begin{bmatrix} f_a \\ f_b \\ f_c \end{bmatrix} = \begin{bmatrix} \cos\theta_r & \sin\theta_r & 1 \\ \cos\left(\theta_r - \frac{2\pi}{3}\right) & \sin\left(\theta_r - \frac{2\pi}{3}\right) & 1 \\ \cos\left(\theta_r + \frac{2\pi}{3}\right) & \sin\left(\theta_r + \frac{2\pi}{3}\right) & 1 \end{bmatrix} \begin{bmatrix} f_q \\ f_d \\ f_n \end{bmatrix} \tag{2.2}$$

In Eqs. (2.1) and (2.2), f denotes the variables such as voltage, current, and flux, and θ_r denotes the electrical angle.

The voltage equation of the PMSM can be expressed as Eq. (2.3) by the dq stationary coordinate system [42].

$$
\begin{aligned}
v_d &= Ri_d + \frac{d}{dt}\left(L_d i_d\right) - \omega_r \psi_q \\
v_q &= Ri_q + \frac{d}{dt}\left(L_q i_q\right) + \omega_r \psi_d
\end{aligned}
\tag{2.3}
$$

where $\psi_q = L_q i_q$, $\psi_d = L_d i_d + \phi$; v_d, v_q is the d-axis and q-axis voltage [V]; i_d, i_q is the d-axis and q-axis stator current [A]; L_d, L_q is the d-axis and q-axis inductance [H]; R is the stator resistance [Ω]; ω_r is the electrical angular speed (or motor synchronous speed) [rad/s], and ϕ is the flux linkage by the rotor magnet [V/rad/s].

The electric torque and the load motion equation generated by the motor are expressed by the following Eqs. (2.4) and (2.5).

$$
T_E = \frac{3}{2} P\left[\phi i_q + \left(L_d - L_q\right) i_d i_q\right] \tag{2.4}
$$

$$
T_E = J\frac{d}{dt}\omega_m + T_F + T_L \tag{2.5}
$$

where T_E is the electric torque [Nm], ω_m is the angular speed of the rotor [rad/s], P is the number of poles, J is the inertia moment of the rotor [kgm^2], T_L is the load torque [Nm], and T_F is the friction torque [Nm]. $T_F = B\omega_m$ where B is the damping coefficient of the rotor [Nm/rad/s].

The vector control of the PMSM controls the phase of the three-phase current to be maintained at a right angle to the rotor flux and the magnetic field rotating at the synchronous speed so that the maximum torque is generated. That is, in normal operation, the d-axis current i_d, which is the magnetic flux component of the stator current, is controlled to be zero. Therefore, if the electric torque is rewritten, the following Eq. (2.6) is obtained.

$$T_E = \frac{3}{2} P \phi i_q \tag{2.6}$$

The motor rotor angular speed ω_m has the relationship delineated in Eq. (2.7) below with the motor synchronous speed ω_r.

$$\omega_m \approx \frac{1}{P} \omega_r \tag{2.7}$$

Finally, the following Eq. (2.8) can be obtained from Eqs. (2.3), (2.4), and (2.5).

$$\begin{aligned} \frac{d}{dt} i_q &= \frac{1}{L_q} \left(v_q - i_q R - P \omega_m \phi \right) \\ \frac{d}{dt} \omega_m &= \frac{1}{J} \left(T_E - T_L - T_F \right) \end{aligned} \tag{2.8}$$

Table 2.1 shows the parameters of the PMSM that is applied.

Table 2.1. PMSM parameters

Stator resistance R [Ω]	0.386
q-axis inductance L_q [H]	0.0000653
Rotor inertia J [kgm^2]	0.00000333
Damping coefficient B [Nm/rad/s]	0.0000016
Number of poles P	4
Flux linkage ϕ [V/rad/s]	0.0092

Figure 2.4 shows the rotor angular speed and the electrical torque response when a step input of 12 V is applied.

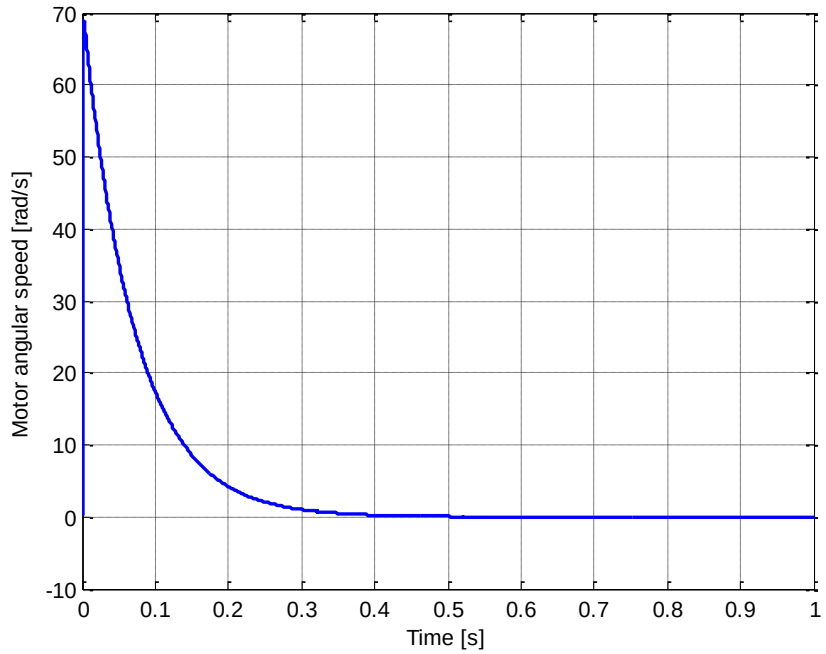

(a)

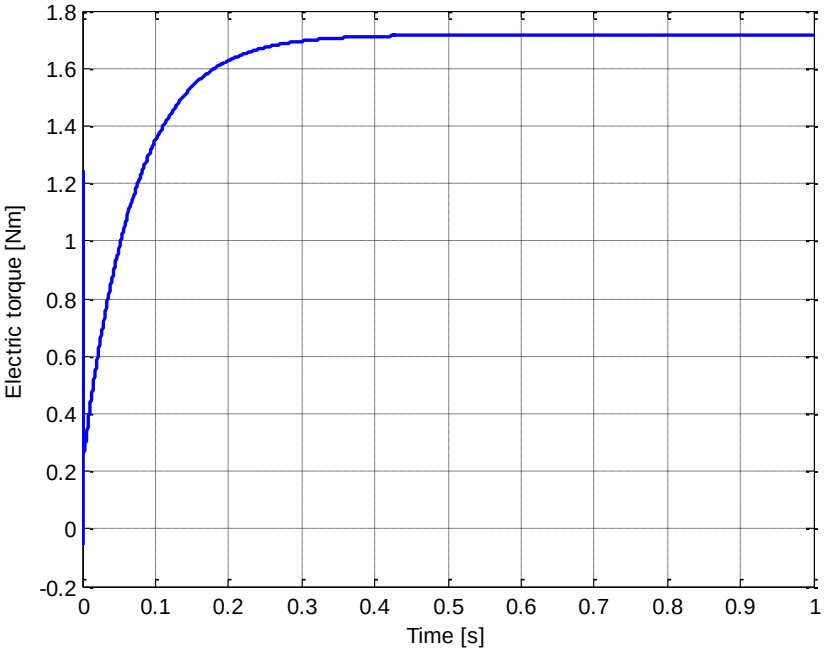

(b)

Fig. 2.4. Simulation results of the PMSM model; (a) Rotor angular speed, (b) Electrical torque

2.2.2 Modeling of the Planetary Gear

The motor used in the EMB system has difficulty supplying torque to achieve sufficient braking force due to the size, installation space problems, and current limit. Therefore, in this study, a planetary gear reducer was used to increase the torque of the motor. The planetary gear reducer occupies a small space in a limited space, thereby making it possible to minimize the mechanism and the apparatus, and to transmit the input shaft torque to the output shaft with high efficiency. The ring gear is a fixed gear, the sun gear is a driving gear, and the carrier is a driven gear in the planetary gear reducer. The output shaft of the motor is connected to the sun gear, and the power is transmitted through the carrier because the ring gear is fixed. Figure 2.5 shows a planetary gear reducer.

Fig. 2.5. Planetary gear reducer

The speed and torque of the reducer carrier are given by the following equations:

$$\begin{aligned} \omega_{red} &= n_g \omega_m \\ T_{red} &= \frac{1}{n_g} T_m \end{aligned} \tag{2.9}$$

where n_g is the reduction gear ratio, ω_{red} is the carrier speed [rad/s], T_{red} is the carrier torque [Nm], and T_m is the sun gear torque (motor load torque).

The EMB system changes in various parts as time passes. In particular, a backlash may occur. If the backlash occurs in the gear reducer, the response of the brake is delayed, which can directly affect the safety of the driver. The backlash changes the speed output of the reducer.

Figure 2.6 shows the output of the planetary gear reducer model. The simulation was performed with a gear ratio of 15:1. The output results are also given in consideration of the backlash.

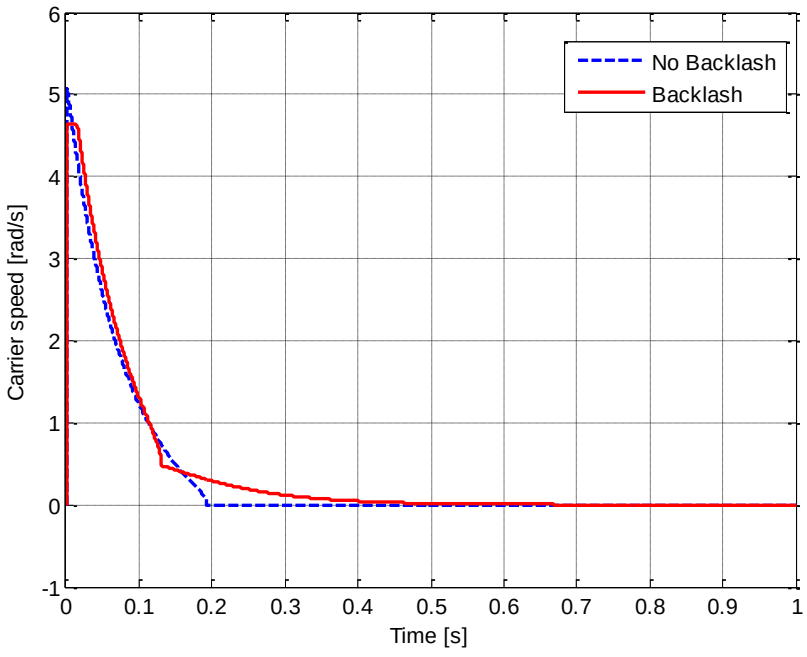

(a)

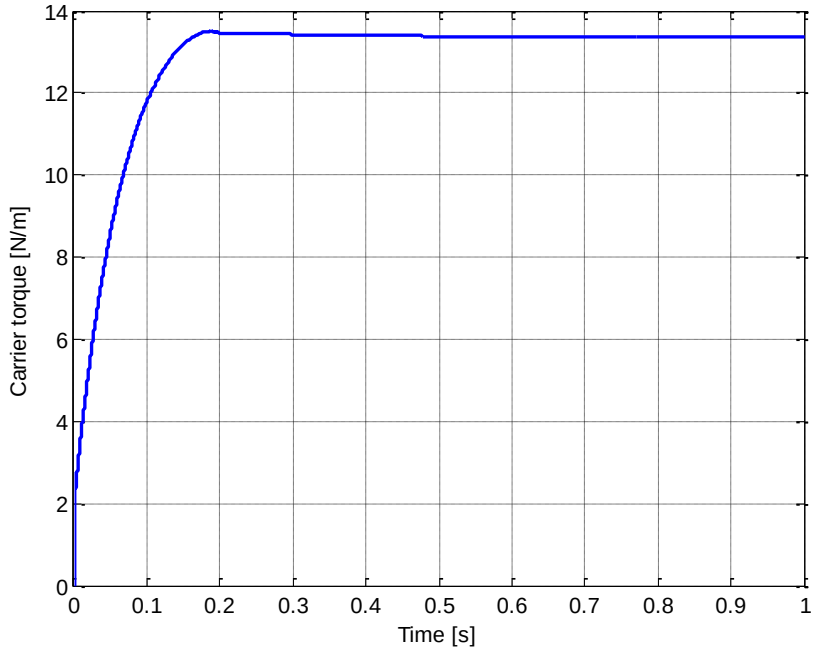

(b)

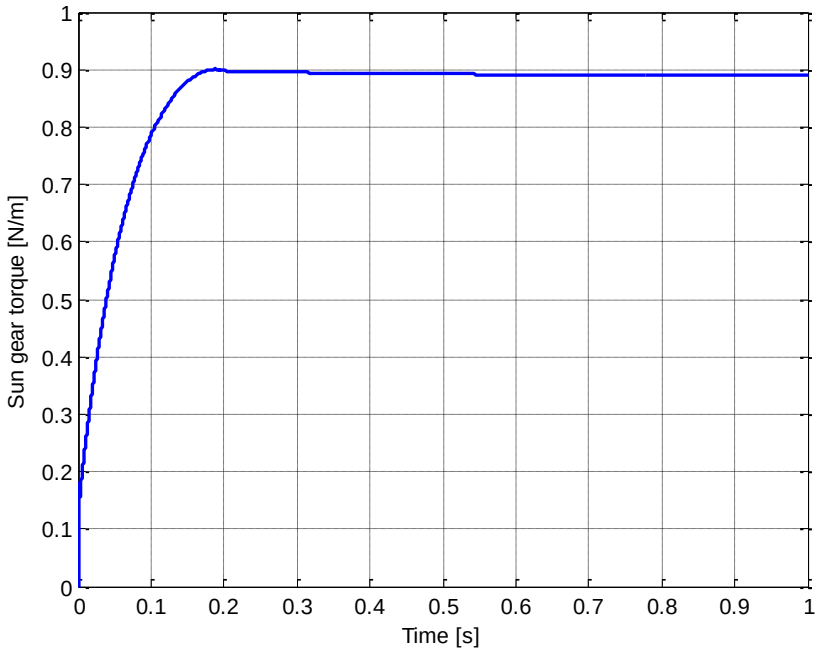

(c)

Fig. 2.6. Simulation results of the planetary gear reducer; (a) Carrier speed, (b) Carrier torque, (c) Sun gear torque

In the section, a friction model based on Coulomb friction, viscous friction, and static friction is applied to accurately express the friction due to the rotational motion of the motor and the reducer [31]. Figure 2.7 shows the friction torque characteristics according to rotational speed considering Coulomb friction, viscous friction, and static friction.

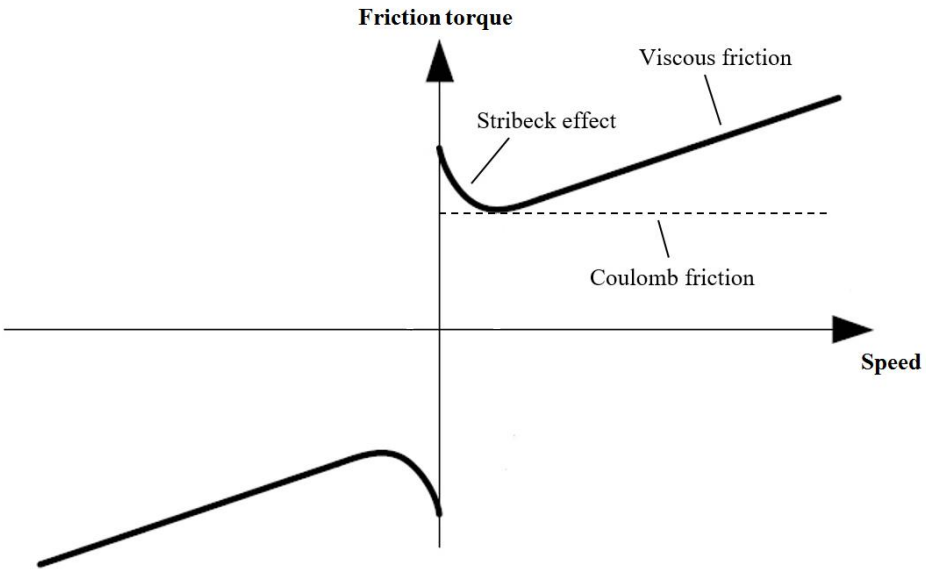

Fig. 2.7. Friction model for the motor and reducer

The friction model is expressed by the following equation.

$$T_F = T_C + (T_S - T_C)e^{-|\omega_{rm}/\omega_s|^{\delta_s}} + B_V\omega_{rm} \tag{2.10}$$

where T_C is the Coulomb friction torque [Nm], T_S is the static friction torque [Nm], B_V is the viscous friction coefficient, and ω_s is the Stribeck velocity [rad/s]. Table 2.2 shows the parameters used in the friction model.

Table 2.2. Friction model parameters

Coulomb friction torque T_C [Nm]	0.2

Static friction torque T_S [Nm]	0.324
Viscous friction coefficient B_V	0.01
Stribeck velocity [rad/s]	8.695

Figure 2.8 shows the simulation results of the friction model. We could get a curve similar to the Figure 2.7.

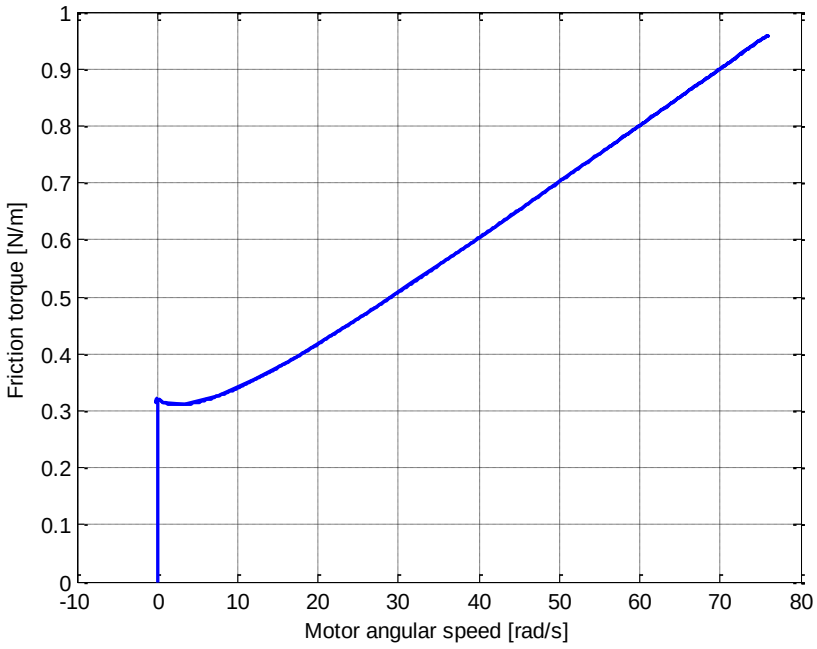

Fig. 2.8. Simulation result of the friction model

2.2.3 Modeling of the Screw Thread

The screw thread is composed of a male screw and a female screw and it converts rotation motion into linear motion. The male screw connected to the reducer carrier is connected to the screw, and the female screw is connected to the piston. The screw converts the rotational motion transmitted from the reducer to the linear motion of the piston, and presses the pad connected to the piston against the disk to obtain the clamping force.

In this study, the screw was modeled as a torsional spring damper. The rotation speed of the screw is defined as follows.

$$\dot{\theta}_{scr} = N\omega_m - \frac{\cos\alpha}{r_{scr}}\dot{x}_{pis} \tag{2.11}$$

where θ_{scr} is the screw rotation speed [rad/s], α is the screw lead angle, r_{scr} is the screw radius, and x_{pis} is the displacement of the piston.

The rotational motion of the screw pushes up the piston on the oblique plane of the thread angle α as shown in Figure 2.9. However, since the piston is fixed in the right and left directions and cannot rotate, only linear motion is performed. The force P acting through the screw and the reaction force Q acting on the piston due to the clamping force act on the piston.

$$\begin{aligned} P &= \frac{k_{scr}\theta_{scr} + b_{scr}\dot{\theta}_{scr}}{r_{scr}} \\ Q &= F_{pis} \end{aligned} \tag{2.12}$$

where k_{scr} is the modulus of elasticity of the screw, b_{scr} is the damping coefficient of the screw, and F_{pis} is the force of the piston.

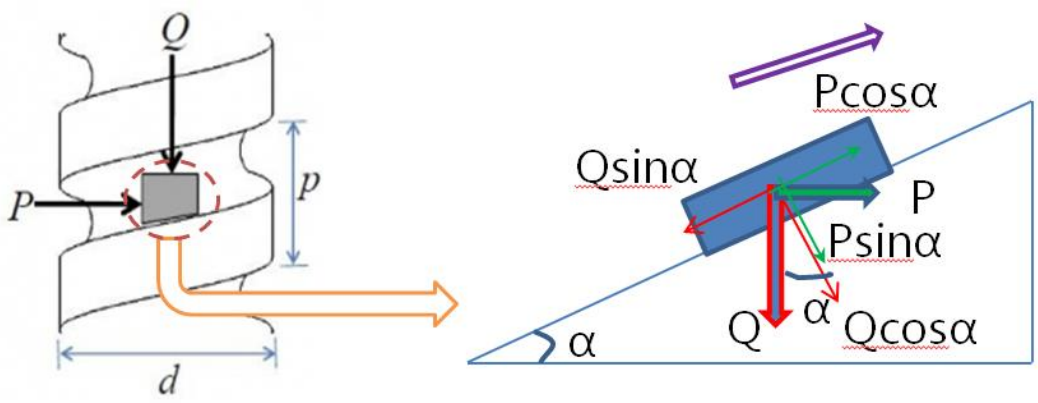

Fig. 2.9. Structure of the screw thread

The forces P and Q acting on the pistons are divided into normal force and vertical force perpendicular to the bevel of the screw.

$$\begin{aligned} V &= Q\cos\alpha + P\sin\alpha \\ N &= Q\sin\alpha + P\cos\alpha \end{aligned} \tag{2.13}$$

The equation of motion of the piston by screw rotation is as follows:

$$M_{pis}\ddot{x}_{pis} + F_F = P\cos\alpha - Q\sin\alpha \tag{2.14}$$

where M_{pis} is the mass of the piston [kg], and x_{pis} is the displacement of the piston at the screw bevel [mm].

Since the direction of the piston in Eq. (2.14) is fixed in the right and left directions and moves in the vertical direction, the displacement of the piston is as follows:

$$x'_{pis} = x_{pis}\frac{p}{2\pi r_{scr}}\cos\alpha = x_{pis}\sin\alpha \tag{2.15}$$

where x'_{pis} is the displacement of vertical direction [mm], and p is the pitch of the screw [mm].

The piston receives the force transmitted from the screw and generates a clamping force to transfer it to the pad. The piston is modeled as a spring damper. The equation of motion is as follows:

$$\begin{aligned} \dot{x}'_{pisc} &= \dot{x}'_{pis} - \dot{x}_{padi} \\ F_{pis} &= k_{pis} x'_{pisc} + b_{pis} \dot{x}'_{pisc} \end{aligned} \tag{2.16}$$

where x'_{pisc} is the displacement of the piston compression, x_{padi} is the displacement of the inner pad, k_{pis} is the elasticity modulus of the piston, and b_{pis} is the damping coefficient of the piston.

Table 2.3 shows the parameters of the screw thread.

Table 2.3. Screw thread parameters

Thread angle α [deg]	3.2
Pitch p [mm]	2.5
Screw radius r_{scr} [mm]	11.5
Screw stiffness k_{scr} [Nm/rad]	4000
Screw friction coefficient b_{scr} [Nm/rad/s]	0.1
Mass M_{pis} [kg]	1

Figure 2.10 shows the vertical force acting on the piston of the screw thread.

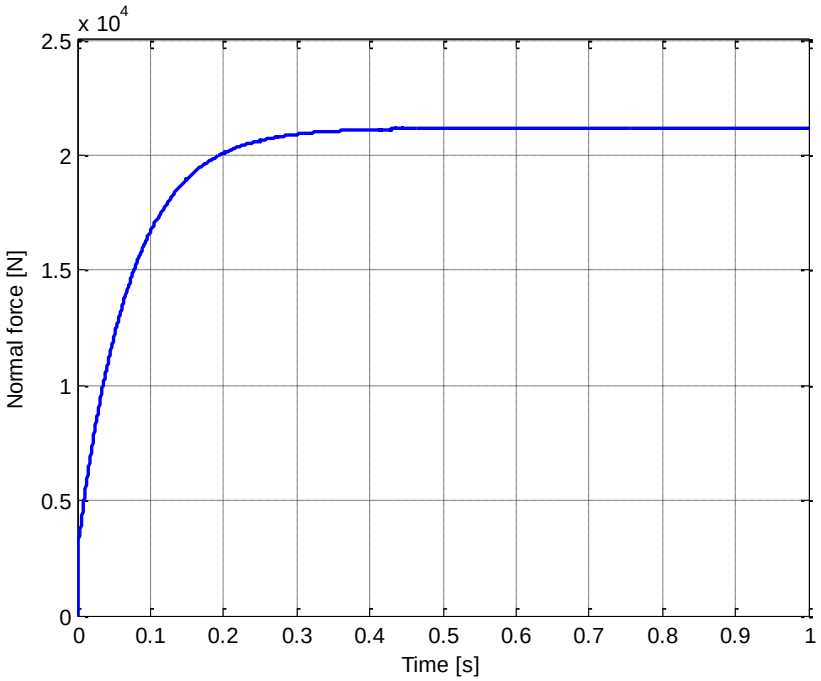

Fig. 2.10. Force acting on the piston

The screw gear converts the rotational motion generated by the motor into a linear motion and pushes the brake pad to generate a clamping force. Now we consider the friction model of the screw thread gear. A friction force is generated which interferes with the movement of the piston due to the vertical force N acting on the piston. The friction force is simulated by the LuGre friction model which simulates the friction characteristics of static and dynamic behavior [43]. Considering the frequently transition between static and dynamic operation range of EMB system, the dynamic LuGre friction model is suitable for our modeling work. All frictions are modeled by LuGre friction model for its ability to capture most characteristics of the friction. The LuGre friction model is modeled the contact of two objects using a function formula according to the deformation of the bristles. When two objects are in contact, the bristles are deformed and a relative velocity is generated between the contact surfaces. The average deformation of the bristles can be modeled by selecting the state variables. The LuGre friction model can be expressed as

$$
\begin{aligned}
&F_c = \mu_c N \\
&F_s = \mu_s N \\
&\dot{z} = v - \sigma_0 \frac{|v|}{g(v)} z \\
&g(v) = F_c + (F_s - F_c) e^{-(v/v_c)^2} \\
&F_F = \sigma_0 z + \sigma_1 v\dot{z} + \sigma_2 v
\end{aligned}
\tag{2.17}
$$

where F_c is the Coulomb friction force, μ_c is the Coulomb friction coefficient, F_s is the static friction force, μ_s is the static friction coefficient, z is the average deformation length of the bristles, v is the relative velocity of the friction surface, $g(v)$ is the function to simulate the nonlinear friction (Stribeck effect), v_c is the Stribeck velocity, σ_0 is the stiffness coefficient of the bristles, σ_1 is the damping coefficient, and σ_2 is the viscous damping coefficient. Table 2.4 shows the parameters applied.

Table 2.4. Friction model parameters of screw thread gear

Coulomb friction coefficient μ_c	0.4
Static friction coefficient μ_s	0.3
Stribeck velocity v_c [m/s]	0.1
Stiffness coefficient σ_0 [N/m]	100000
Damping coefficient σ_1 [Ns/m]	1000
Viscous coefficient σ_2	0.01

The accurate parameters of the LuGre friction model require sophisticated experiment equipment and procedures, which is not available in our case. Therefore, the parameters of the LuGre friction model are derived from the design specifications. The relationship between screw efficiency and friction can be expressed as

$$\eta = \frac{1-\mu_c \tan\alpha}{1+\mu_c / \tan\alpha} \tag{2.18}$$

where η is the screw efficiency. If we choose the screw efficiency, then the screw Coulomb friction coefficient can obtained by Eq. (2.18). It is assumed that the influence of viscous friction in the EMB system is almost negligible.

Figure 2.11 shows the force output of the LuGre friction model of the screw thread gear.

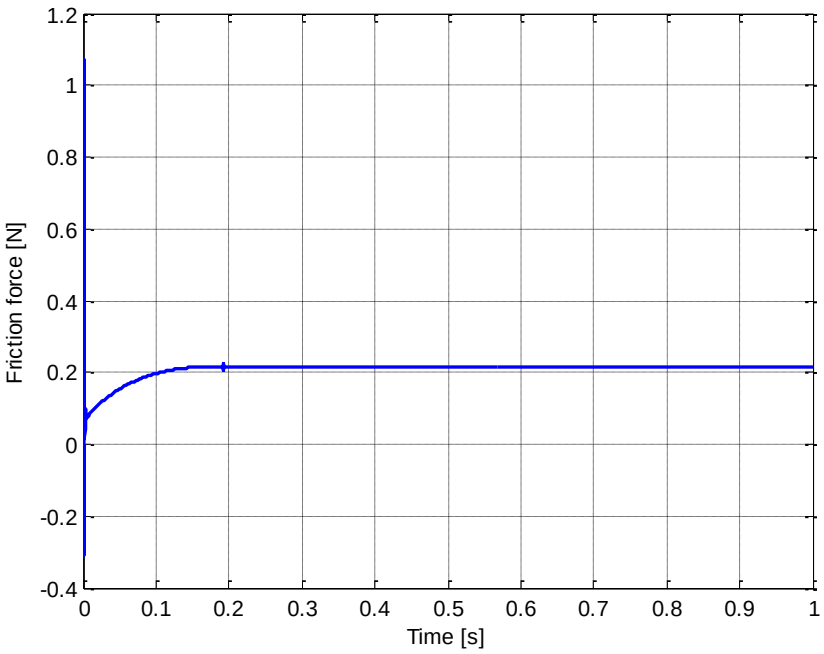

Fig. 2.11. Simulation result of LuGre friction model of the screw thread gear

2.2.4 Modeling of the Caliper

The disk brake consists of pads and disk caliper housing. The operating principle is

as follows. During operation, the force of the motor rotation causes the inner pad to come into close contact with the disk through the piston, and the piston cannot advance any further. When the caliper housing connected to the motor body is pushed back by the reaction of the piston, the outer pad is pulled to squeeze the pad onto the disk. As a result of this action, the outer pad and the inner pad are simultaneously pressed against the disk and the braking force due to friction is obtained. The caliper is modeled by a mass, spring, and damper. The equation of motion is as follows:

$$\begin{aligned} &M_{cal}\ddot{x}_{calc} + b_{cal}\dot{x}_{calc} + k_{caliper}x_{calc} = b_{pis}\dot{x}'_{pis} + k_{pis}x'_{pis} \\ &x_{calc} = x_{cal} - x_{pado} \\ &F_{cal} = b_{cal}\dot{x}_{calc} + k_{cal}x_{calc} \end{aligned} \tag{2.19}$$

where M_{cal} is the mass of the caliper, x_{cal} is the displacement of the caliper, x_{calc} is the compression displacement of the caliper, b_{cal} is the damping coefficient of the caliper, k_{cal} is the elasticity modulus of the caliper, and F_{cal} is the force of the caliper.

Table 2.5 shows the applied caliper parameters.

Table 2.5. Caliper parameters

Caliper stiffness k_{cal} [N/m]	2.5×10^{11}
Caliper friction coefficient b_{cal} [Ns/m]	10000
Caliper mass M_{cal} [kg]	5.5

2.2.5 Modeling of the Pads

The pads are located on both sides of the disk and the clamping force is generated to compress the disk by the force transmitted from the piston of the EMB and the force transmitted from the caliper. An air gap is maintained between the pad and the disk to prevent

drag torque when releasing the brake. Therefore, the clamping force is not generated until the pad moves a distance as much as the gap.

The spring-damper model is given by the following equations (the inner pad):

$$\begin{aligned} &x_{padi} < x_{gap} \Rightarrow M_{pad}\ddot{x}_{padi} = F_{pis} \\ &x_{padi} \geq x_{gap} \Rightarrow x'_{padi} = x_{padi} - x_{gap} \\ &M_{pad}\ddot{x}'_{padi} + b_{pad}\dot{x}'_{padi} + k_{pad}x'_{padi} = F_{pis} \end{aligned} \tag{2.20}$$

where M_{pad} is the mass of the pad, x_{padi} is the displacement of the inner pad, b_{pad} is the damping coefficient of the pad, k_{pad} is the elasticity modulus of the pad, and x_{gap} is the gap distance between the pad and disk.

The equation of motion of the outer pad is given by the following equations:

$$\begin{aligned} &x_{pado} < x_{gap} \Rightarrow M_{pad}\ddot{x}_{pado} = F_{cal} \\ &x_{pado} \geq x_{gap} \Rightarrow x'_{pado} = x_{pado} - x_{gap} \\ &M_{pad}\ddot{x}'_{pado} + b_{pad}\dot{x}'_{pado} + k_{pad}x'_{pado} = F_{cal} \end{aligned} \tag{2.21}$$

where x_{pado} is the displacement of the outer pad, and F_{cal} is the force by the caliper.

The clamping force F_{cl} is expressed by the sum of the inner pad force by the piston and the outer pad force by the caliper.

$$\begin{aligned} F_{padi} &= k_{pad}x'_{padi} + b_{pad}\dot{x}'_{padi} \\ F_{pado} &= k_{pad}x'_{pado} + b_{pad}\dot{x}'_{pado} \\ F_{cl} &= F_{padi} + F_{pado} \end{aligned} \tag{2.22}$$

where F_{padi} is the inner pad force and, F_{pado} is the outer pad force. If x'_{padi} and x'_{pado}

are equal, the clamping force can be expressed as follows:

$$F_{cl} = 2\left(k_{pad}x'_{pad} + b_{pad}\dot{x}'_{pad}\right) \tag{2.23}$$

Table 2.6 shows the parameters of the applied pad.

Table 2.6. Pad parameters

Pad stiffness k_{pad} [N/m]	3×10^{7}
Pad friction coefficient b_{pad} [N/m/s]	2×10^{8}
Mass M_{pad} [kg]	0.3

Figure 2.12 shows the displacement of the pad and the output of the clamping force. We set the initial air gap of 0.2 mm. From Figure 2.12, it can be confirmed that the displacement of pad of about 0.2 mm and the clamping force accordingly.

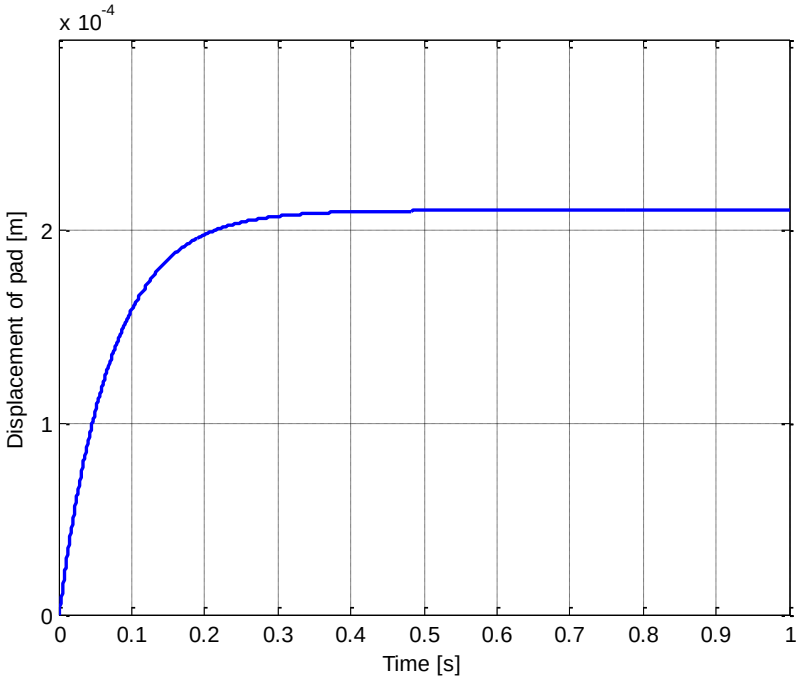

(a)

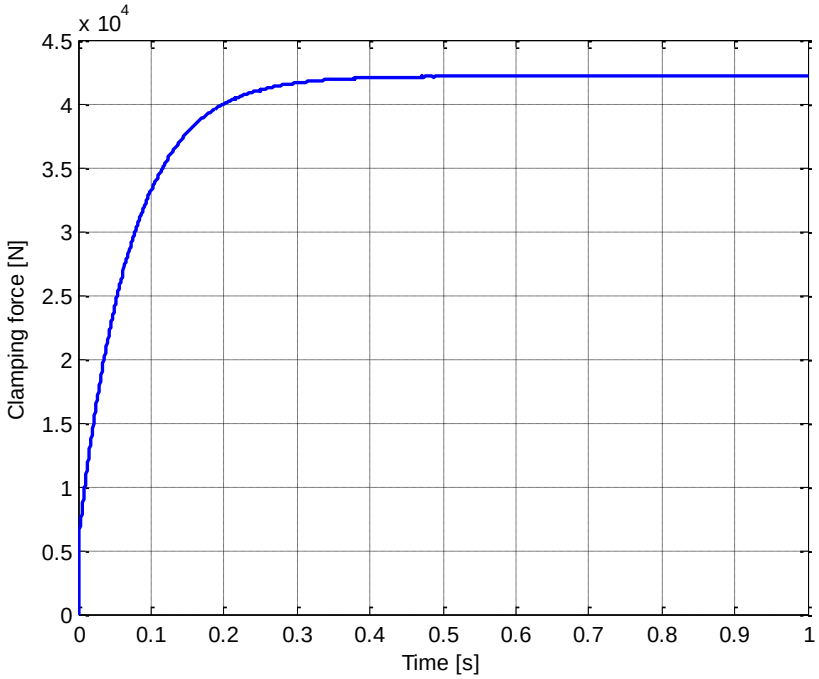

(b)

Fig. 2.12. Simulation results of the pad model; (a) Displacement of the pad, (b) Clamping force

2.3 Control of EMB System

The EMB controller in this thesis has the control structure as shown in Figure 2.13. The central ECU transmits the required clamping force corresponding to the driver's input to the controller ECU via CAN communication. The clamping force controller in the controller ECU controls the actuator to precisely follow the received clamping force. The speed controller outputs the current command using the speed command received from the host controller such as the clamping force controller and the speed measurement obtained through differential calculation of the electrical angular. The current controller converts the three-phase current of the motor to the dq-axis and outputs the voltage required to rotate

the rotor using the current measurement and the current command received from the speed controller. The output voltage is applied to the motor via the inverter. To improve each controller response, integral anti-windup is incorporated as well as feed-forward compensation of the back-EMF and Coulomb friction. The anti-windup technique used the inverse calculation method. This method reduces the integral term by suppressing the accumulation of the integrator by multiplying the difference between the pre- and post-limit values of the controller output by the gain. We referred to the Ref. [8, 44, 45, 46, 47] to implement the cascaded PI controller.

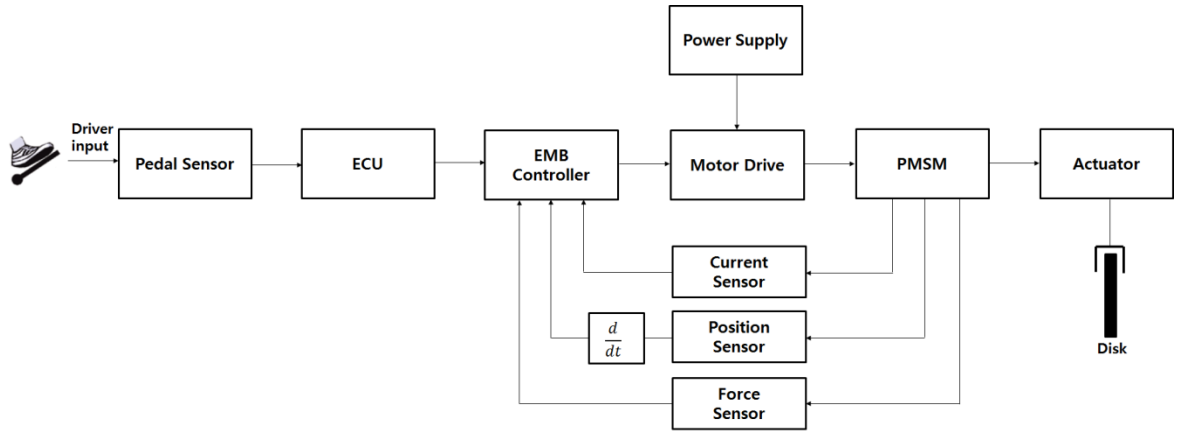

Fig. 2.13. Block diagram of EMB control system

2.3.1 Design of the Current Controller

The current controller uses the PI controller type. The input of the controller is the dq-axis current command and the current measurement output from the speed controller. Assuming that the back-EMF of the motor is forward-compensated, the current controller is as shown in Figure 2.14.

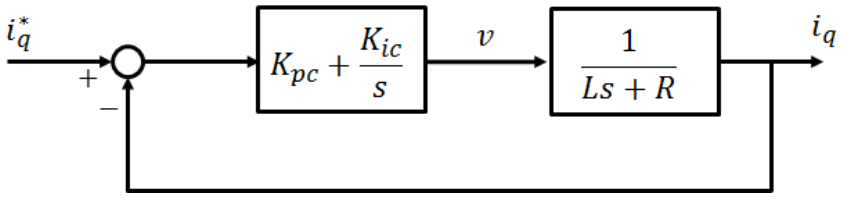

Fig. 2.14. PI current controller

The dq-axis current measurement is obtained by dq-axis transformation the phase current of the motor. The current controller outputs a voltage required to rotate the rotor in accordance with the current command and the current measurement. It is modulated through a PWM inverter to allow the motor to apply the appropriate three-phase voltage. The maximum torque is generated in the PMSM when the magnetic rotor and the rotating frame are maintained at a right angle with the three-phase current control. In this case, the d-axis current, i_d, is set to be zero.

The gain of the current controller depends on the electrical constants L, R, and the bandwidth ω_{cc} of the motor. The equation is expressed as follows.

$$\begin{aligned} K_{pc} &= L\omega_{cc} \\ K_{ic} &= R\omega_{cc} \end{aligned} \tag{2.24}$$

In Eq. (2.23), the bandwidth is selected as 10 kHz. The gain of the integral anti-windup controller is selected as $1/K_{pc}$.

2.3.2 Design of the Speed Controller

The speed controller uses the PI controller type. The input of the controller is the speed command transmitted via CAN communication and the speed measurement measured

through the position sensor. Figure 2.15 illustrates a control system with a PI speed controller.

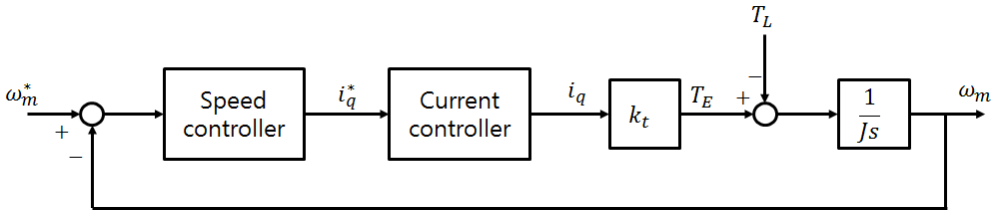

Fig. 2.15. PI speed controller

The current controller designed in the previous section is regarded as the 1st order time delay type with bandwidth ω_{cc}, and the friction coefficient was neglected by including the load torque. The speed measurement is calculated from the electrical angle of the rotor. However, it is sensitive to the system noise which contains high-frequency components, because it is obtained through the derivative of the rotor electric angle. Therefore, a properly designed low-pass filter is applied to remove noise. The output of the speed controller is the torque component current command, and the magnetic flux component current reference is always set to zero unless a weak field operation is required.

The gain of the speed controller depends on the motor's mechanical constant J, torque constant k_t, and bandwidth ω_{cs}. This equation is expressed as follows.

$$K_{ps} = \frac{J\omega_{cs}}{k_t}$$
$$K_{is} = \frac{J\omega_{cs}^2}{5k_t} \tag{2.25}$$

The bandwidth ω_{cs} of Eq. (2.24) is usually chosen to be less than 1/5 of the bandwidth of

the current controller. The gain of the integral anti-windup controller is selected as $1/K_{ps}$.

2.3.3 Design of the Force Controller

The clamping force controller is a PI controller, and its output determines the input of the speed controller. The force controller controls the clamping force between the pad and the disk. Since the force controller determines the command input of the speed controller, the output of the force controller should not exceed the maximum speed of the motor. The gain tuning is appropriately performed based on the proportional gain thus obtained.

$$\begin{aligned} K_{pf} &= \frac{\omega_{\max}}{F_{\max}} \\ K_{if} &= 0.001; \end{aligned} \tag{2.26}$$

where ω_{max} is the maximum speed of the rotor, and F_{max} is the maximum clamping force. The small integral gain is chosen to eliminate the steady state error.

2.3.4 Simulation Results

During application with no initial air gap, the EMB must obtain a clamping force of 30 kN with less than 5% overshoot and a rising time of 0.15 second. The results of clamping force control are shown in Figures 2.16-2.18. Typical inputs, specifically, step, absolute sine wave of 0.5 Hz, and pulse wave of 1 Hz, are taken into account.

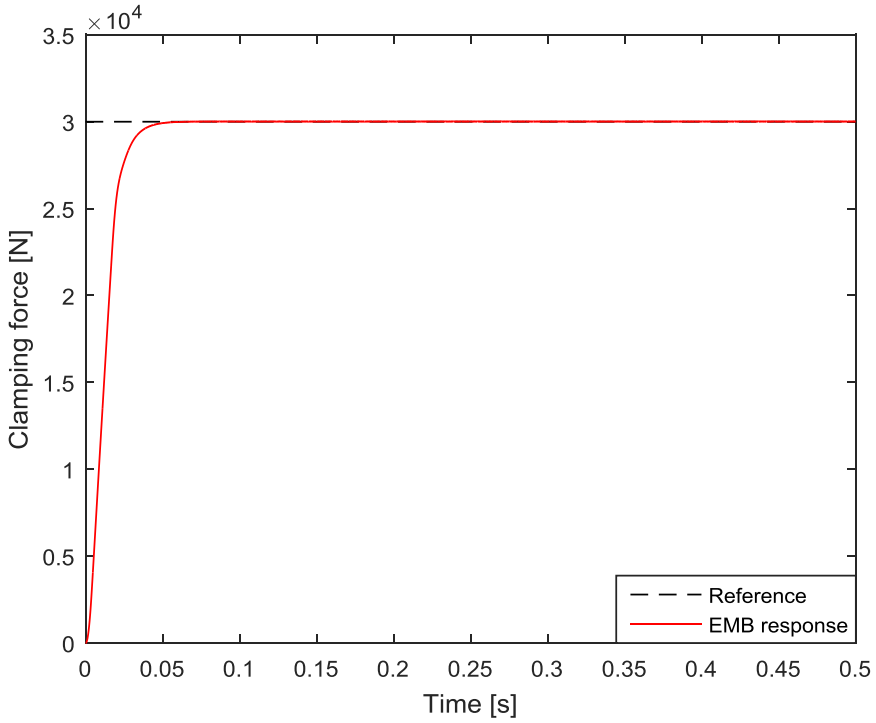

Fig. 2.16. 30 kN step response

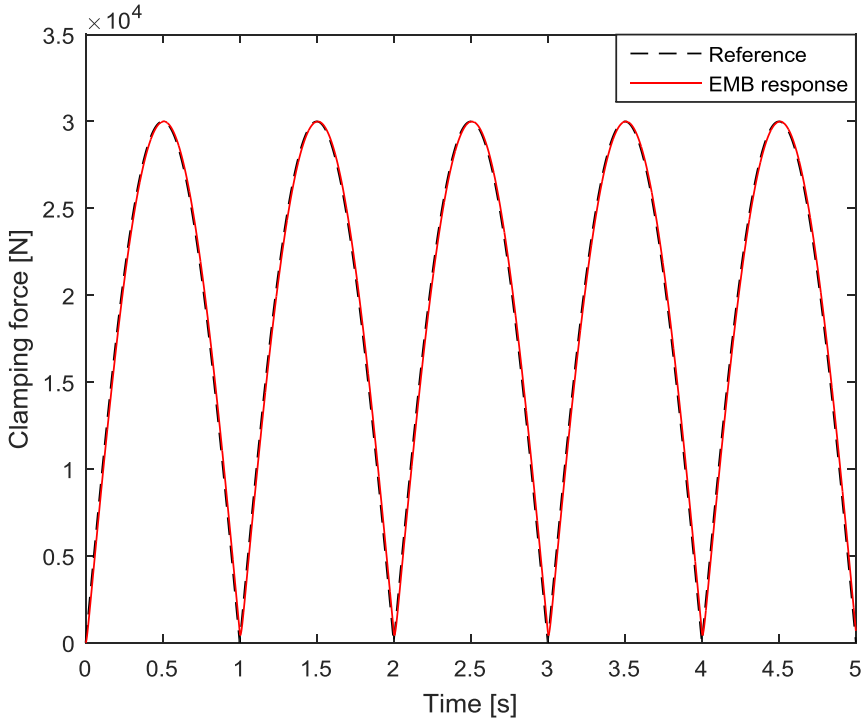

Fig. 2.17. 0.5Hz |sine| wave response

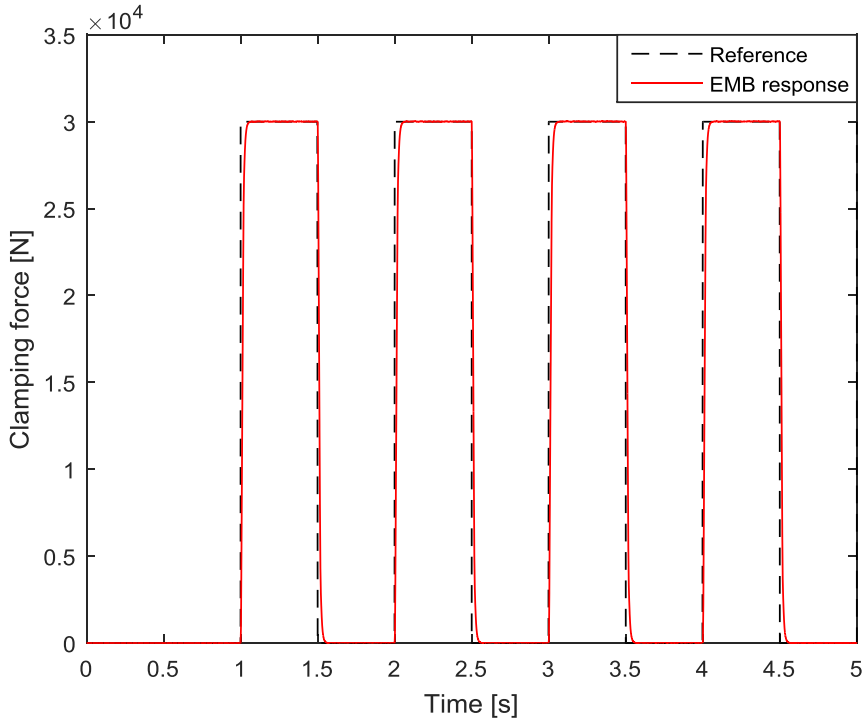

Fig. 2.18. 1 Hz pulse wave response

The results show that the EMB cascaded PI controller can regulate the clamping force accurately.

2.3.5 Experiment for Evaluation of Simulation Results

This chapter briefly describes the developed EMB system, and verifies the model by comparing the EMB simulation results and real EMB output.

Figures 2.19-2.20 show the prototype and components of the EMB. First, the power is generated by a power source applied to the electric motor. The torque of the motor is measured through the current sensor built into the inverter and the speed of the motor is measured through the encoder. In the Gearhead, the power input from the motor is lowered by the reduction ratio and the torque is increased. In the Gear 1, the increased torque of re-

ducer is transmitted to Gear 2. In the Gear 2, the torque transmitted through the Gear 1 is transmitted to the Gear 3 engaged with the screw shaft. In the Gear 3, the torque input through the Gear 2 is transmitted to the screw. In the screw, the rotary motion is converted into a linear motion and the piston is moved in accordance with the rotation of the Gear 3 coupled with the shaft. The clamping force generated by the piston is measured in the load cell (clamping force sensor).

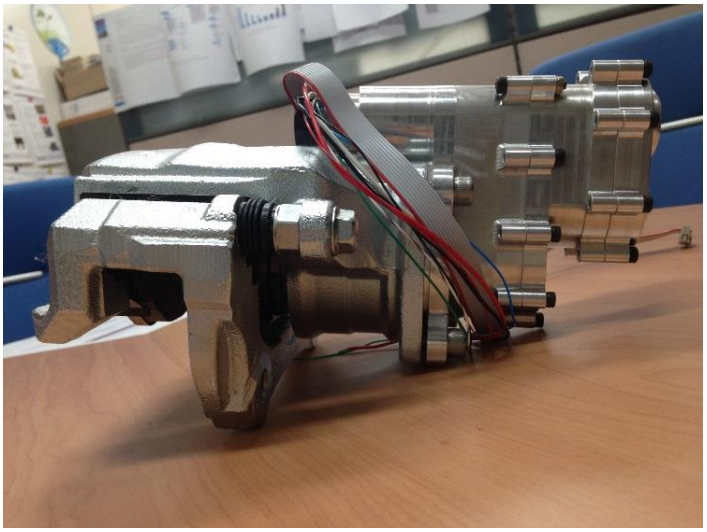

Fig. 2.19. EMB prototype

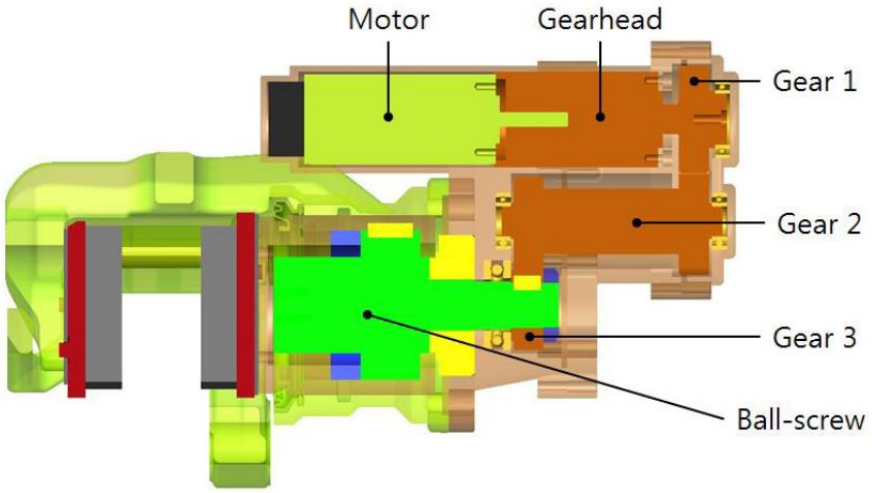

Fig. 2.20. Components of the EMB

Figure 2.21 shows the concept of the operation principle described above.

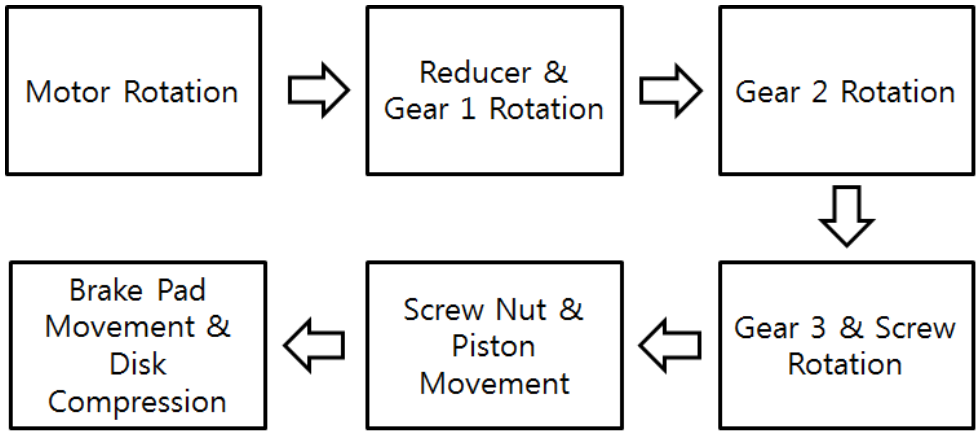

Fig. 2.21. Concept diagram of the EMB operation

The EMB system specifications are listed in the Table 2.7.

Table 2.7 Specification of the EMB system

Electric motor	Nominal voltage 48 V Nominal speed 15,000 rpm Nominal current 3.68 A Nominal torque 92.9 mNm
Gear ratio	86:1
Weight	8.3 kg
Size	85 mm × 130.5 mm × 187.5 mm
Stroke	29 mm
Pad lining area × thickness	60 cm^2 × 12 mm
Required clamping force	24 kN or more

The hardware platform for EMB controller consists of a control unit that receive commands from the host controller to generate necessary control pulses and an inverter unit that switches power supplied to the PMSM according to the control pulses. We used a Freescale MPC5643L microcontroller unit, and the detailed configuration is as follows.

- CAN, FlexRay, Analog command with host controller interface support
- DAC 4ch as interface for monitoring
- Motor quadrature encoder (A, B, Z) interface and hall sensor signal input I/O support

The inverter is configured to supply the required 5 V to each logic circuit through a linear regulator by supplying the FET driver with step down to 15 V through the buck converter power circuit of the operating power 48 V. Figure 2.22 and Table 2.8 show the control board and connectors, respectively. Figure 2.23 shows the configuration of the EMB and control system.

Fig. 2.22. Control board

Table 2.8 Connectors of control board

Connector	Reference number
JTAG port	P1
Inverter PWM I/O	P2
Power & command I/O	P3
Encoder & Hall sensor input	P4

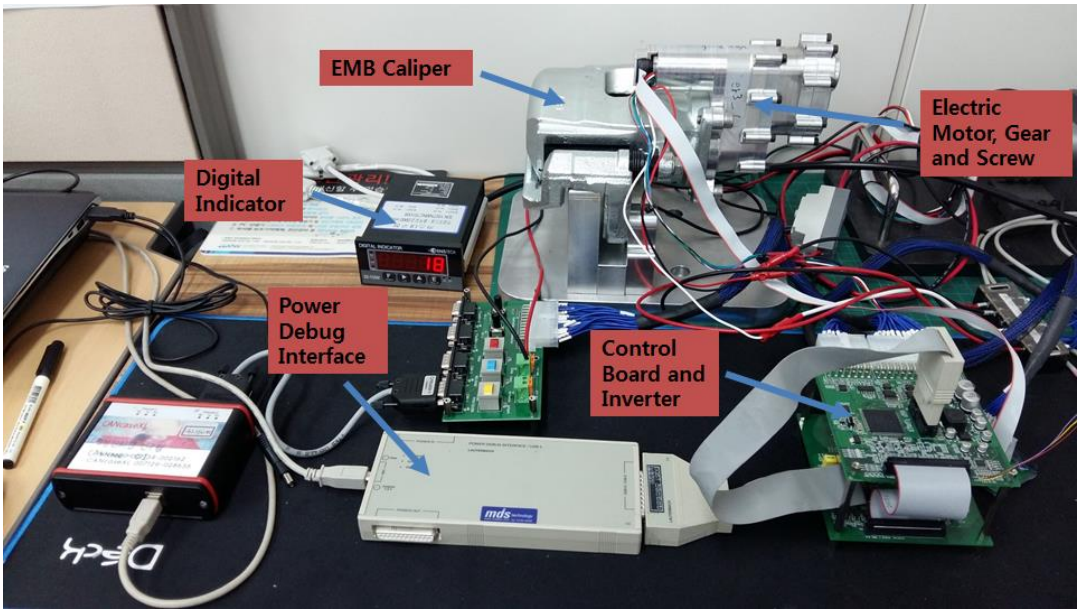

Fig. 2.23. Configuration of the EMB control system

The closed loop control of the EMB model is compared to the clamping force measurement data obtained by the real controlled EMB system. The reference, simulated and real clamping force are shown in Figure 2.24. We can see that the controlled clamping forces are tracking the reference fairly well. Figure 2.25 shows the simulated and real motor currents. As the clamping force increases to 24 kN, the instantaneous motor current increases in the reverse direction and then decreases due to the static friction force of the gear and screw, and the kinetic frictional force due to rotation.

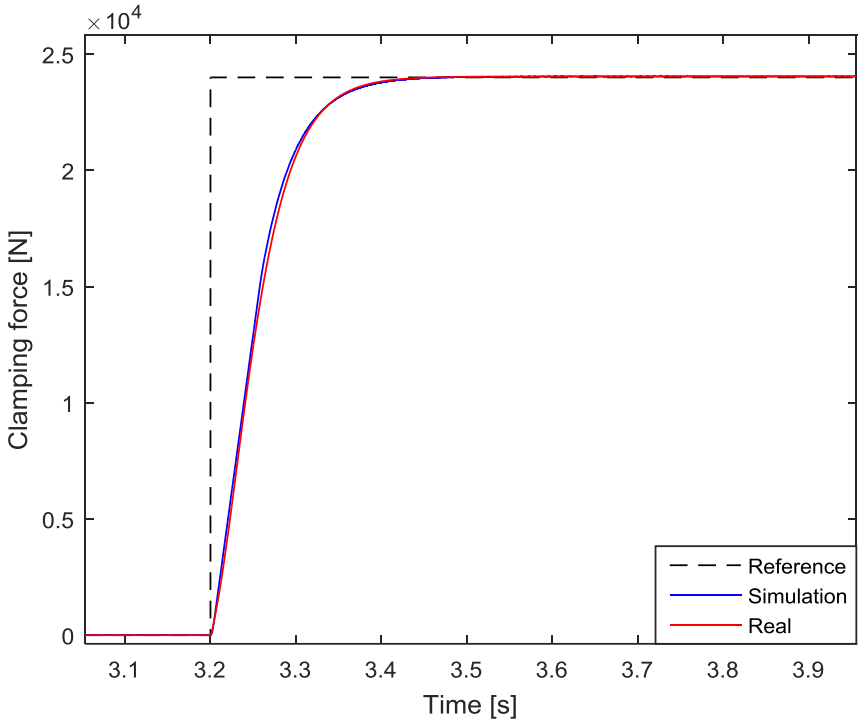

Fig. 2.24. Simulated and real clamping force

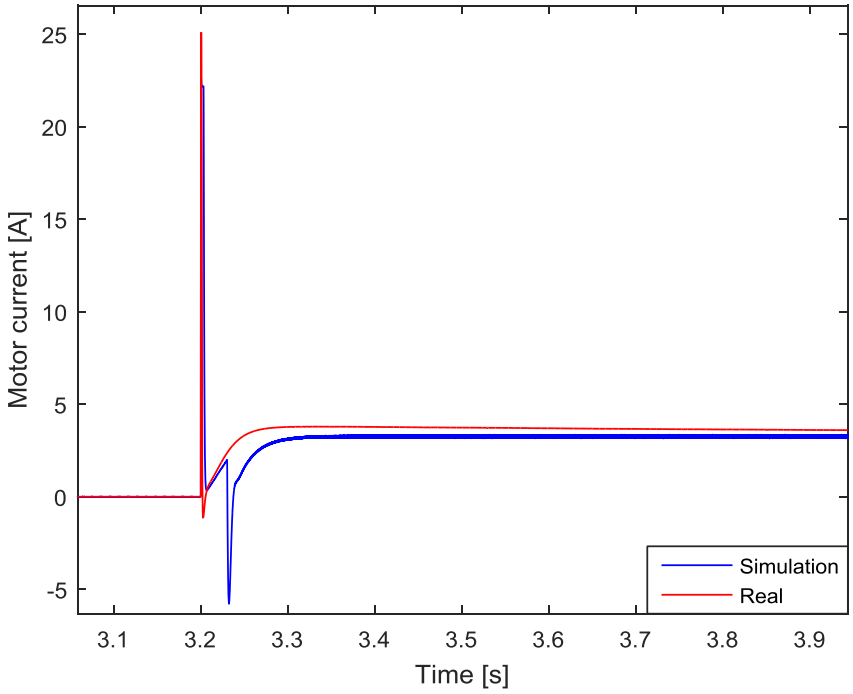

Fig. 2.25. Simulated and real motor currents

As we can notice in Figures 2.24 and 2.25, there are some discrepancies between the simulated and real measured value, which means our EMB model and development works need further adjustment. These discrepancies relate to a common factor as gear and screw thread frictions. As the friction increase, the motor current required increases accordingly. In conclusion, the peak and steady state difference of motor current is resulted from the friction.

2.4 Conclusions

In this chapter, the mathematical modeling and control system of an EMB used as a braking actuator in a BBW systems was designed and its performance was examined through simulations. The PMSM used in the EMB actuator, planetary reduction gear, screw, inner/outer pad, and caliper was modeled and a cascaded PI controller was designed. The equations of motion of each component are derived based on Newton's second law. The EMB model also captures the important effects such as nonlinear stiffness of caliper and pad are considered, and friction of the system which is modeled by the LuGre friction model. The EMB model can be used sufficiently as a simulator. The developed model will be integrated with the full vehicle dynamics and the ABS logics in the future.

III. Nonlinear Identification of Electronic Brake Pedal System Using Hybrid GMDH and Genetic Algorithm

3.1 Introduction

The X-by-wire (XBW) system is a relatively new technology being increasingly implemented in modern automobiles. The XBW system is an automotive system that interprets the driver's inputs and executes appropriate commands to produce desired vehicle behavior, typically via a microprocessor based control system. For fault tolerance, a typical XBW system consists of redundant sensors, actuators, microprocessors, and communication channels. In the XBW equipped vehicle, there are no mechanical or hydraulic connections between the driver's input interface (e.g., throttle, brake, steering) and the target vehicle system [48, 49].

The brake-by-wire (BBW) system, a type of XBW, was first introduced in the Mercedes Benz SL series in 2001 [50]. However, that BBW system was decommissioned and removed from the vehicle a few years later due to a number of field problems. Work on the electro-mechanical brake (EMB) in the BBW was being pursued in the late 1990's by a number of automotive companies, including Bosch, Continental, and TRW [51]. However, issues related to reliability still remain and must be addressed before these systems can be used in an automobile [13].

To ensure the BBW system reliability, accurate modeling of the real system is an important step. Models can be used for the EMB analysis, to gain a better understanding of the system. The models also allow us to predict and simulate the system's behaviors. Furthermore, models are necessary for designing new processes, analyzing existing processes,

designing controllers, optimizations, supervision, and fault detection and diagnosis. For these purposes, various system identifications have been applied in many fields to model and predict the behavior of complex nonlinear systems based on given input/output data.

In this chapter, first of all, the developed BBW systems were described. Based on the systems, brake pedal sensor signals were measured. Secondly, a hybrid GMDH/GA was applied to identify the system for virtual sensor. We then evaluated the performance of the hybrid GMDH/GA as a system identification tool.

3.2 Related Works

Many soft computing approaches for identifying and modeling the nonlinear systems have been proposed. Most of these methods require large amounts of data to estimate the parameters of the model in higher order systems [52]. For example, neural networks and fuzzy logics are used to identify and predict the nonlinear systems based on empirical raw data. Especially, the neural networks are one of the most powerful methods in various fields that have been widely employed in recent years [53, 54]. However, when using such methods, the nonlinear dynamics are not explicitly expressed as a mathematical model. Therefore, a GMDH was first developed by A. G. Ivakhnenko as a multivariate analysis method for complex systems modeling and identification [55]. The main idea in GMDH is to build an analytical function in a feed-forward network based on a quadratic node transfer function whose coefficients are obtained using regression technique. Note that once the analytical GMDH model has been found, application of this model is very quick and cheap. In addition, the GMDH identification is often “black boxes”, and they are especially valuable when the underlying physics is complex or uncertain while there is plenty of data to devel-

op a virtual sensor [56]. Kim et al. [57] had applied the GMDH to the analysis of the stopping maneuver of the driver in the new three-dimensional driving simulator. Consequently, GMDH provides an effective approach for the identification of higher order nonlinear systems. However, the GMDH needs a suitable optimization method to find the best network architecture. For the best network architecture, the GA is arranged in a new approach, to design the whole architecture of the GMDH. This provides the optimal number of neurons in each hidden layer and the connectivity configuration needed to find the optimal set of appropriate coefficients of quadratic expressions to model the system.

3.3 Configuration of Developed BBW Systems

The developed BBW system architecture is proposed and shown in Figure 3.1. It consists of the EMB modules, the electronic brake pedal system, a communication network, main and local electronic control units (ECUs) and power supplies. The EMB actuators are based on the electric motors and a mechanism that applies force to friction pads. The detailed BBW systems are mainly comprised of four types of elements:

1) Electronic Control Units (ECUs),

2) Sensors – pedal sensor, hall sensor, and encoder,

3) Actuator – electric motor, reduction gear, screw and caliper,

4) Communication network – CAN and FlexRay.

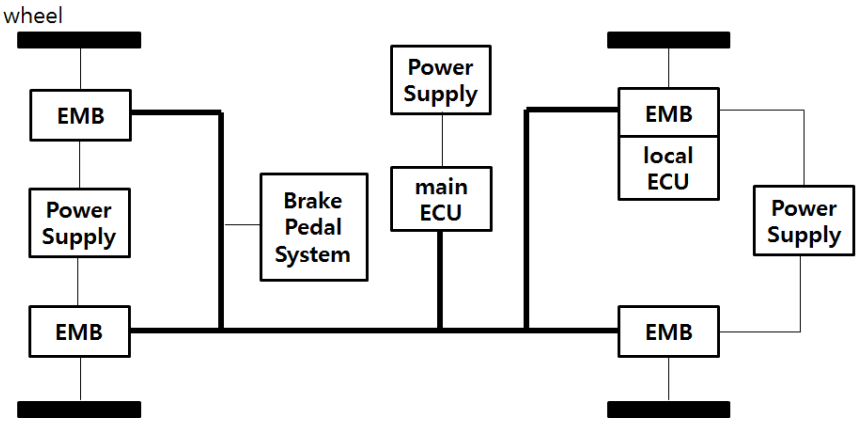

Fig. 3.1. Architecture of developed BBW systems

Figure 3.2 illustrates the block diagram of the developed BBW systems. Once the driver inputs a brake command to the system via the brake pedal, a clamping force command signal is generated by the main ECU. This command signal is sent to the EMB local ECU and display via a communication network. The controller uses the clamping force command as a reference input. The controller provides drive control commands for a motor drive module. This module controls three-phase currents for the brake actuator which is a PMSM, energized by a 42 V power source. In addition to tracking its reference, the controller also controls the current and position of the PMSM.

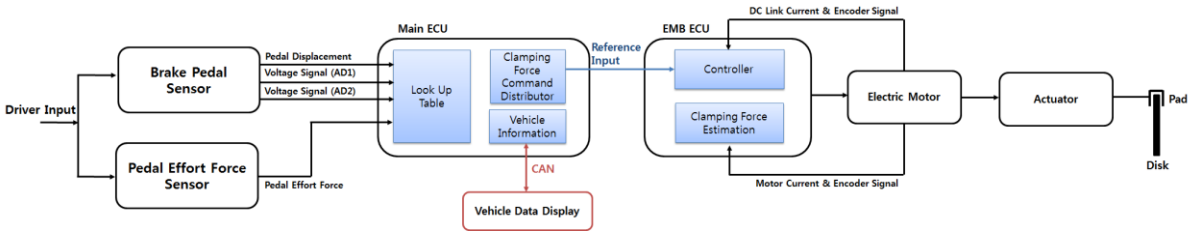

Fig. 3.2. Block diagram of the developed BBW systems

3.4 Review of System Identification Based on Soft Computing

In this chapter, the architecture and features of neural network, fuzzy, and GMDH are briefly described.

3.4.1 Neural Networks

One of the most widely used non-linear system identification is based on the application of artificial neural networks (ANNs) [58]. The structure and functionality of ANNs has been motivated by the architecture of the human brain. In other words, ANNs are designed to make a computer have human learning ability. ANNs show the ability to learn from the environment in an interactive way. They also have remarkable abilities of learning, recall, generalization, and adaptation to changes of the operating environments [25].

ANNs consist of several interconnected processing elements arranged together with weighted connections. These elementary units are called neurons. Each neuron in the network operates by taking the sum of the weighted inputs and passing the results through a non-linear activation function. Figure 3.3 shows the general architecture of neural networks. Network learning is performed through training or exposure to a set of input and output data where the training algorithm adjusts the weights iteratively [26].

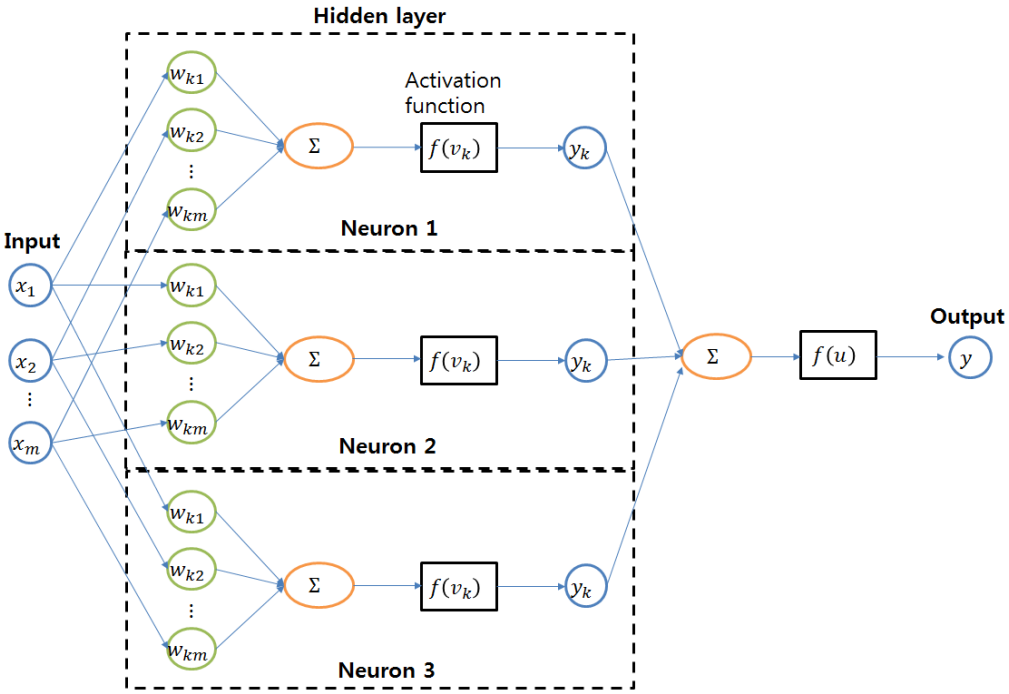

Fig. 3.3. Neural network architecture

The system identification of neural networks is defined as the procedure used to find the inputs and output relationship of a dynamic model. This step involves four steps: collection of high quality input/output data, selection of a network structure, training of the network and validation of the trained network. The quality of the trained network is related to the quality of the training data that can be obtained by either an experiment of the real system to be modeled or from a simulation using a mathematical model of the system. To create a meaningful model of the identified system, the training data must include information about the overall operating range of the system. Then, the network architecture should be selected. The next steps involve training and evaluating the model, respectively. A commonly used verification method is to investigate prediction errors by running sets of test data on the trained model [59].

ANNs has several properties that make them an attractive tool for system identification. However, the successful application of the ANNs in the system identification depends

on a proper selection of the neural network architecture. For the multi-layer perceptron (MLP) of the classical ANNs, the problems are the selection of number of layers and the number of neurons in a particular layer. If the obtained network does not satisfy pre-defined requirements, a new network structure is selected and the parameter estimation is repeated again. An arbitrary selection of the ANNs structure can cause the model uncertainty [58].

3.4.2 Fuzzy Model

The human brain interprets the information of the ambiguous and uncertain stimuli perceived by the senses. Fuzzy is a systematic calculation method to deal with this unclear information. Fuzzy logic, introduced by Zadeh in 1962, emulates the way in which the human brain deals with concepts such as uncertainty, vagueness, and imprecision [22]. It allows human to express and process relationships in form of rules. The rules of fuzzy models are generally determined by an expert who knows the system very well or by numerical methods. A typical fuzzy model consists of a rule-base module that contains a number of fuzzy if-then rules, a database that defines the membership functions (MFs) of the fuzzy sets used by the fuzzy rules, a decision-making subsystem that performs the inference operations on the rules, a fuzzification module that transforms inputs to degrees of membership to different fuzzy sets and finally, a defuzzification module that transforms the fuzzy results into an output [60]. Figure 3.4 shows the block diagram of a typical fuzzy inference system.

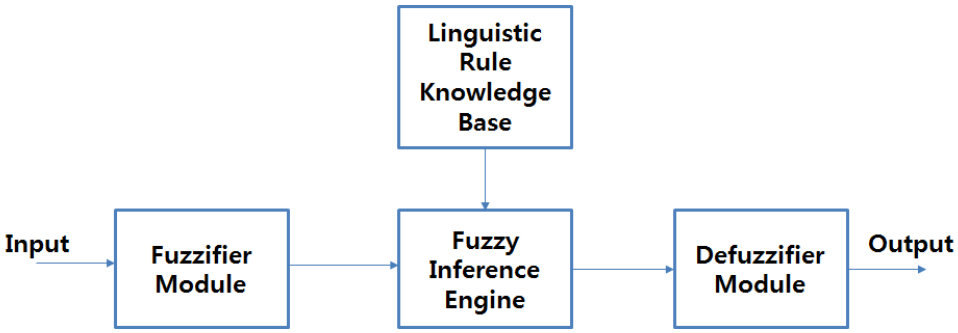

Fig. 3.4. Block diagram of fuzzy inference system

3.4.3 Group Method of Data Handling

In general, the complex multivariate modeling has difficulties in determining the structure of a model by selecting variables among the many input and output variables, and the amount of data required for estimation becomes large when the number of the coefficients of the estimation method increases. To overcome this drawback, A. G. Ivakhnenko proposed a GMDH algorithm [55]. GMDH is a multilayered network with a certain structure determined through training. Not only is the nonlinear dynamics are expressed as a mathematical model, the polynomials are characterized by higher order terms without instability problems [61, 62]. It aims to find relationships between one output and a frequently large set of possible inputs. The network determines which of the possible inputs can actually be associated with the system being identified. Therefore, the network is built up layer by layer during training. Each layer has a neuron with only two inputs; the output of each neuron is a quadratic function of its both inputs. The parameters of the quadratic functions are obtained using linear regression analysis. Before adding a new layer, the previous layer is trained. During this training, for each unique combination of two inputs, a neuron is trained and on the basis of a certain selection criteria, only the best performing neurons are selected. Then, a new layer is added, and the whole procedure of training is performed

again on this new layer. Adding new layers are done if some stopping criteria are achieved [30, 63, 64].

The Table 3.1 shows the historical trend of soft computing. A detailed description of GMDH algorithm and its application in the electronic brake pedal system identification will be provided in the following chapter.

Table 3.1. Historical trend of soft computing

	Neural Networks	**Fuzzy**	**Other Methodologies**
1950s	Perceptron (1957)		
1960s	Adaline, Madaline (1960)	Fuzzy sets (1965)	GMDH (1968)
1970s	Back-propagation (1974), Cognition (1975)	Fuzzy controller (1974)	Genetic algorithm (1970)
1980s	Self-organizing map (1980), Hopfield net (1982)	TSK model (1985)	Artificial life immune modeling (1985)
1990s		Neuro-fuzzy (1990), ANFIS (1991), CAN-FIS (1994)	Genetic programming (1990)

3.5 Application of Hybrid GMDH/GA to the Electronic Brake Pedal System

In this section, we describe for a hybrid GMDH/GA and propose the schematic of brake pedal system identification.

3.5.1 GMDH Algorithm

The general connection between the inputs and output variables can be expressed by

a complicated polynomial series in the form of the Volterra series, known as the Kolmogorov-Gabor polynomial [29, 30]:

$$y = a_0 + \sum_{i=1}^{m} a_i x_i + \sum_{i=1}^{m}\sum_{j=1}^{m} a_{ij} x_i x_j + \sum_{i=1}^{m}\sum_{j=1}^{m}\sum_{k=1}^{m} a_{ijk} x_i x_j x_k + \cdots \tag{3.1}$$

where x is the input to the system, m is the number of inputs and a are coefficients. For most applications the quadratic forms for only two variables, which are called partial descriptions, are used in the form to predict the output as follows:

$$y = a_0 + a_1 x_i + a_2 x_j + a_3 x_i x_j + a_4 x_i^2 + a_5 x_j^2 \tag{3.2}$$

To obtain the value of the coefficients a for each model, a system of Gauss normal equations is solved. The coefficient of nodes in each layer is expressed as follows.

$$A = \left(X^T X \right)^{-1} X^T Y \tag{3.3}$$

where

$$Y = \left[y_1, y_2, \ldots, y_m \right]^T,$$

$$A = \left[a_0, a_1, a_2, a_3, a_4, a_5 \right],$$

$$X = \begin{bmatrix} 1 & x_{1p} & x_{1q} & x_{1p}x_{1q} & x_{1p}^2 & x_{1q}^2 \\ 1 & x_{2p} & x_{2q} & x_{2p}x_{2q} & x_{2p}^2 & x_{2q}^2 \\ \vdots & \vdots & \vdots & \vdots & \vdots & \vdots \\ 1 & x_{mp} & x_{mq} & x_{mp}x_{mq} & x_{mp}^2 & x_{mq}^2 \end{bmatrix}.$$

The main function of GMDH is based on the forward propagation of a signal through nodes of the net similar to the principal used in classical neural nets. Every layer consists of simple nodes each of which performs its own polynomial transfer function and passes its output to nodes in the next layer. The basic steps involved in the GMDH modeling are as follows [57, 65]:

Step 1: Select input variables $X = \{x_1, x_2, \dots, x_m\}$. Divide the available data into training and checking data sets. Before applying the algorithm, the inputs and output are normalized.

Step 2: Construct $k = \binom{m}{2} = m(m-1)/2$ new variables $Z = \{z_1, z_2, \dots, z_k\}$ in the training data set and construct the regression polynomial for the first layer by forming the quadratic expression which approximates the output y.

Step 3: Identify the contributing nodes at each hidden layer according to the value of the root mean square error (RMSE). Eliminate the least effective variable by replacing the columns of X (old data) by the new columns of Z.

Step 4: The GMDH algorithm is carried out by repeating Step 2 and 3 of the algorithm. When the errors of the checking data in each layer stop decreasing, the iterative computation is terminated.

The network constructed using the self-organizing GMDH algorithm is shown in Figure 3.5 [66].

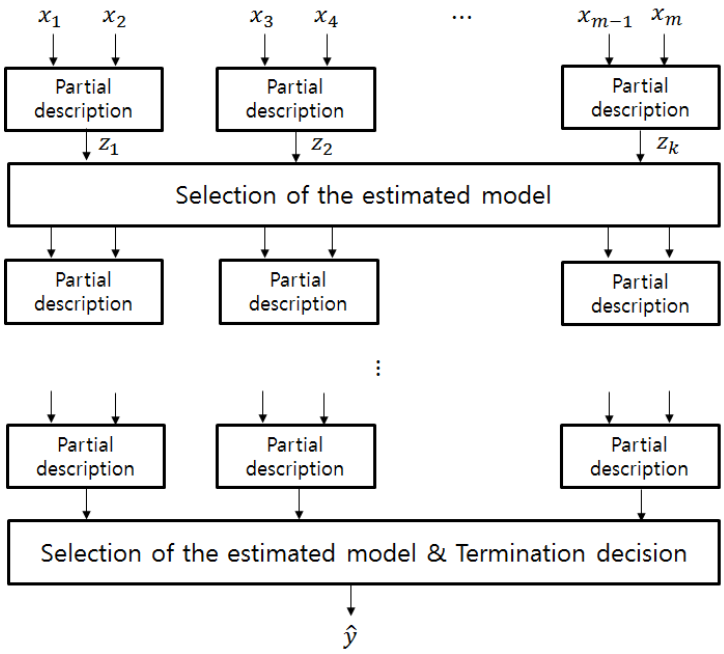

Fig. 3.5. Self-organizing GMDH algorithm

3.5.2 Hybrid GMDH/GA based on Genome Representation

The GA is commonly used in the training of neural networks in terms of associated weights or coefficients, and has successfully performed better than traditional gradient-based techniques. In most GMDH algorithms, the neurons in each layer are only connected to neurons in the adjacent layer. Taking advantage of this feature, it is possible to present a simple encoding scheme for the genotype of each individual in the population [67, 68].

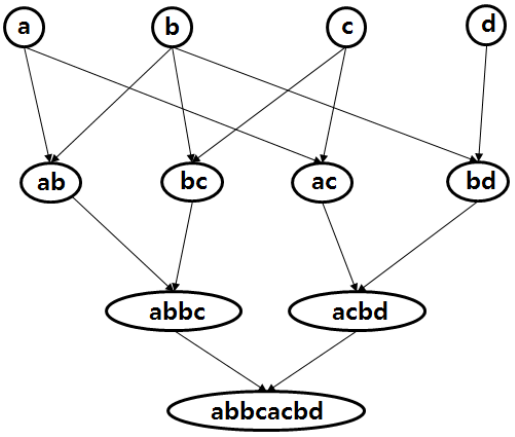

Fig. 3.6. Genome representation

In Figure 3.6, neurons in the first hidden layer are connected to the output layer by directly going through the second hidden layer. The genome or chromosome representation, which shows the topology of a GMDH, simply consists of a symbolic string composed of an alphabetic representation of the input variables [28]. In this encoding scheme, each input variable is assigned an alphabetic name, and a chromosome is a string of concatenated sub-strings of these alphabetic names of inputs. It should be noted that such repetition occurs whenever a neuron passes through some adjacent hidden layers and connects to another neurons in the next 2^{nd} , 3^{rd} ,… following hidden layer. In this encoding scheme, the number of repetitions of that neuron depends on the number of passed hidden layers l, and is calculated as 2^l.

3.5.3 Proposed Scheme of Electronic Brake Pedal System Identification

In the BBW equipped vehicle, the brake pedal sensor is safety-critical component, and this failure will disrupt the vehicle's operation and endanger human lives [69]. The main ECU must always be informed of the driver's intentions to brake or to stop the vehi-

cle, and fault data from the pedal sensor is a serious problem for vehicle control systems. For this reason, the design of a these vehicles need to include safeguards that prevent abnormal behavior. General solutions to this problem include providing hardware redundant sensors, and applying a fail-safe mechanism. In addition to the complete loss of sensor information, the ECU may also suffer from an intermittent data loss. This may result from an instantaneous short circuit or disconnection, a communication network fault, or a sudden increase in noise. To address these problems, we introduce a system identification approach based on hybrid GMDH/GA as the virtual sensor [70, 71]. The following Figure 3.7 shows the proposed scheme of the electronic brake pedal system identification. In order to model and identify the brake pedal system, the following sensory information is captured as inputs: pedal effort force [kgf], voltage signal AD1 [V], voltage signal AD2 [V], and pedal displacement [%]. The output is the clamping force command [N]. The residual analysis will conduct the fault diagnosis function; in other words, it will be used with the measured data given by the pedal behavior to compare with the results obtained using the estimated data generated by the hybrid GMDH/GA.

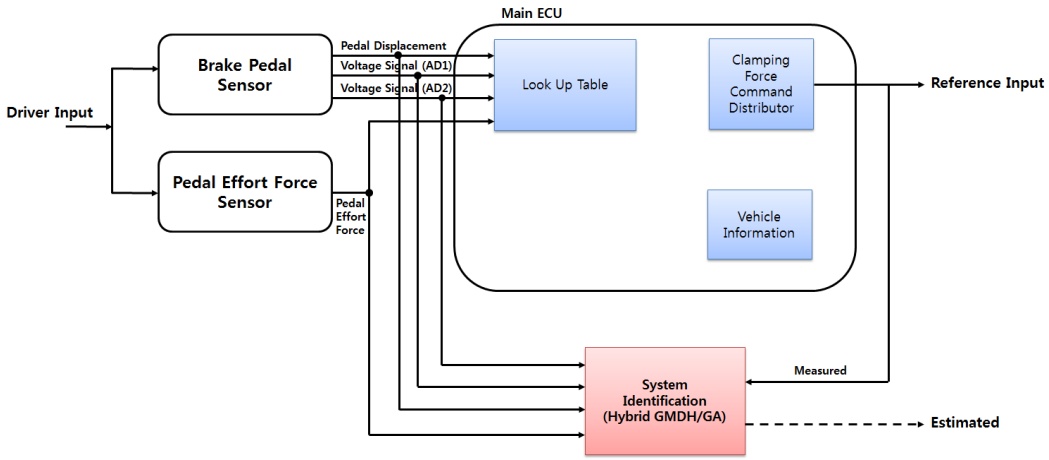

Fig. 3.7. Proposed scheme of electronic brake pedal system identification using hybrid GMDH/GA

3.6 Experimental Results

3.6.1 Experimental Setup

For the system identification, tests were made on the BBW systems. Our BBW systems are composed of brake pedal, pedal effort force sensor, ECUs, wheel speed sensors, and EMBs as Figure 3.8 and 3.9. In the EMB system, the electric motor is of the PMSM type maxon EC 4-pole motor with ratings of 200 W and 15,000 rpm and ensures that the required clamping force command (up to 30 kN) can be achieved. Figure 3.10 shows the data sheet of the maxon EC 4-pole motor [72].

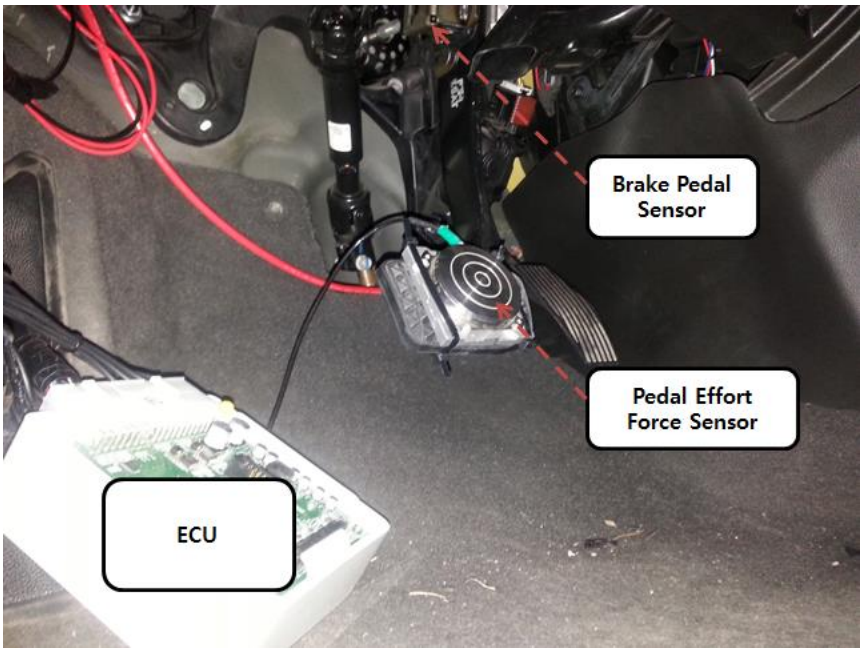

Fig. 3.8. Electronic brake pedal system in real car

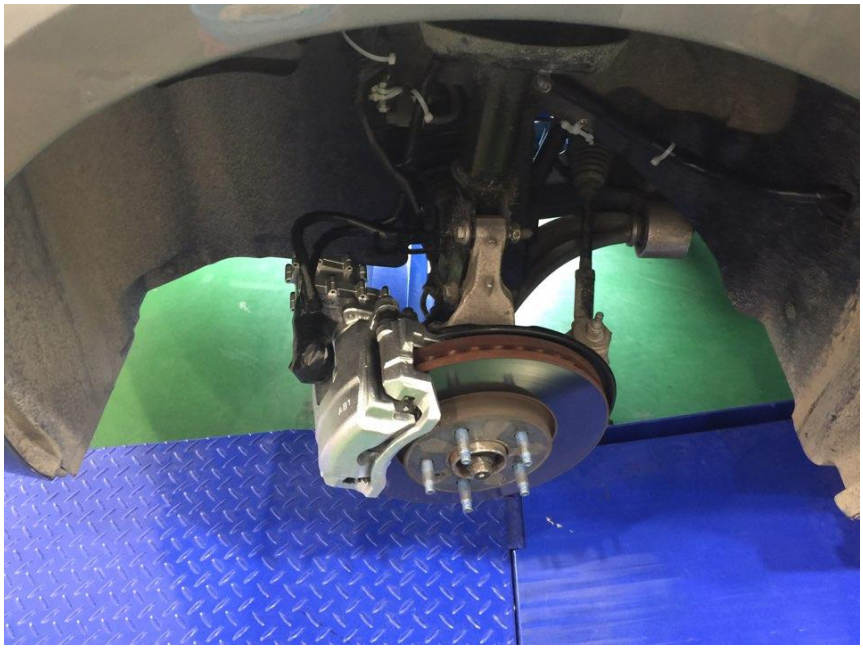

Fig. 3.9. Front wheel equipped with EMB

	Motor Data		305013	305014	305015
	Values at nominal voltage				
1	Nominal voltage	V	24	36	48
2	No load speed	rpm	16700	16700	16500
3	No load current	mA	728	485	356
4	Nominal speed	rpm	16100	16200	16000
5	Nominal torque (max. continuous torque)	mNm	94.6	94.2	92.9
6	Nominal current (max. continuous current)	A	7.58	5.03	3.68
7	Stall torque	mNm	3220	3510	3430
8	Stall current	A	236	171	124
9	Max. efficiency	%	89	90	90
	Characteristics				
10	Terminal resistance phase to phase	Ω	0.102	0.21	0.386
11	Terminal inductance phase to phase	mH	0.016	0.037	0.065
12	Torque constant	mNm/A	13.6	20.5	27.6
13	Speed constant	rpm/V	700	466	346
14	Speed/torque gradient	rpm/mNm	5.21	4.78	4.83
15	Mechanical time constant	ms	1.82	1.67	1.69
16	Rotor inertia	gcm²	33.3	33.3	33.3

Fig. 3.10. Maxon EC 4-pole motor data sheet

The parameters of interest in this four-input one-output system, which both affect the performance of the clamping force command are the pedal effort force [kgf], voltage signals (AD1 [V] and AD2 [V]) and pedal displacement [%]. We used the DEWETRON

monitoring system in order to acquiring data [73]. DEWETRON software is widely used as modular data acquisition equipment in automotive, aerospace and heavy industry. The monitoring system updates in-vehicle information received from each ECU via CAN and overall EMB status information in real-time as Figure 3.10. Accordingly, there were a total of 100,000 experimental data considering four input parameters, as shown in Figure 3.11. Out of which 70,000 data points are randomly selected for the training data set while the remaining 30,000 data points are selected for the checking data set. We choose the sampling interval of 0.2 ms.

Fig. 3.10. DEWETRON monitoring system in real car

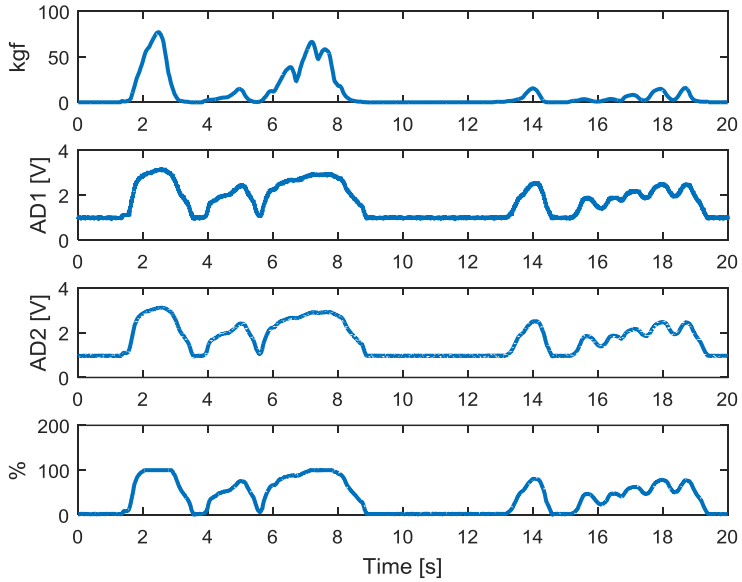

Fig. 3.11. Experimental data; pedal effort force [kgf] (first), voltage signal AD1 [V] (second), voltage signal AD2 [V] (third), and pedal displacement [%] (fourth)

In the hybrid GMDH/GA, a population size of 20 was employed together with a crossover probability of 0.9 and a mutation probability of 0.1 in a generation number of 6 and number of hidden layer of 4. The hybrid GMDH/GA was implemented on a PC with an Intel Core CPU 1.5 GHz and RAM 8 GHz. We can construct the structure of the network, which is shown in Figure 3.12.

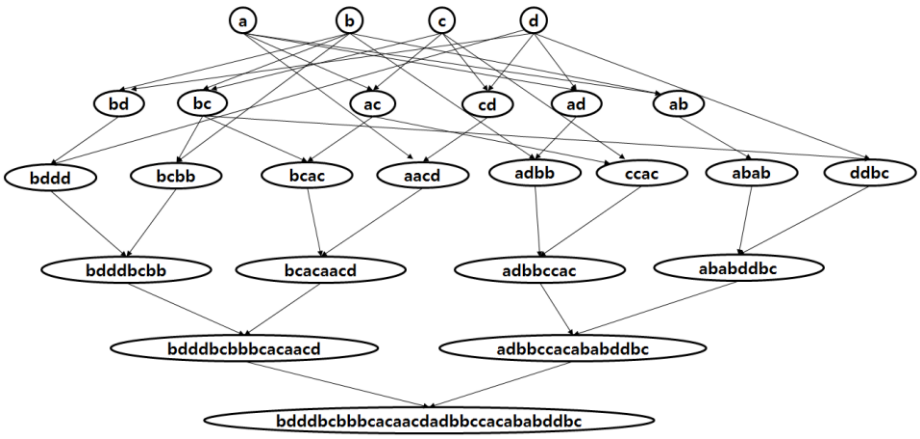

Fig. 3.12. Network structure of the brake pedal system identification using hybrid GMDH/GA

3.6.2 Comparison of Results and Discussions

The well-known criterion for comparing the different identification methods is the root mean square error (RMSE) and correlation coefficients (R) of the predicted outputs from each model. The reason for using these criterions is that we need to measure the quality of the models and also the predictability of the models.

The neural network was trained for 1000 epochs using the Levenberg-Marquart back-propagation algorithm with a learning rate of 0.001 and an error goal of 0.01. Figure 3.13-3.15 shows the results for the measured, estimated output data and residual errors for neural network, GMDH, and hybrid GMDH/GA identification, respectively. When a random stepwise and sinusoidal clamping force command is applied, the estimated values follow the target values, which show close agreement with the measured values. Especially, the figures show that proposed hybrid GMDH/GA identification offers good estimation performance.

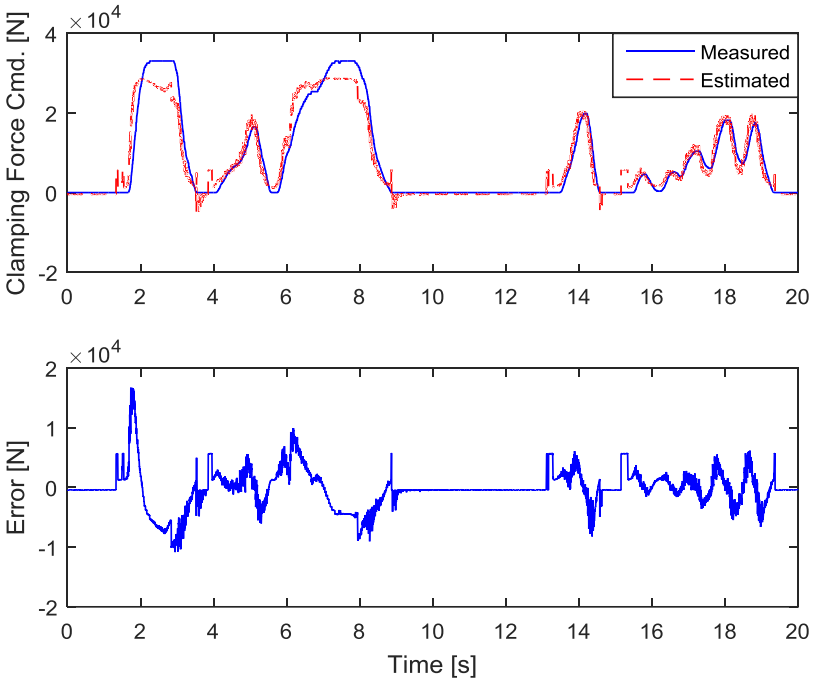

Fig. 3.13. Neural network identification results

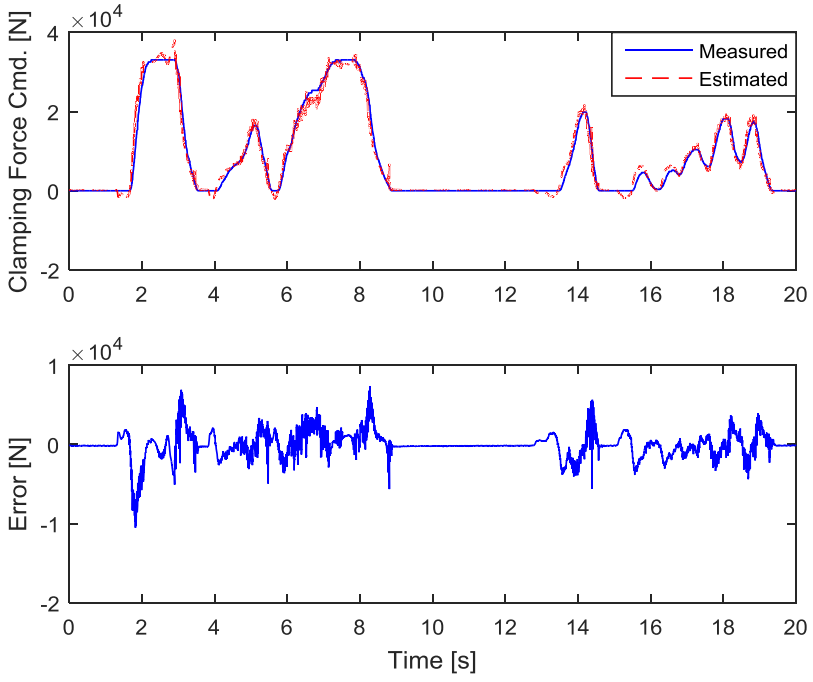

Fig. 3.14. GMDH identification results

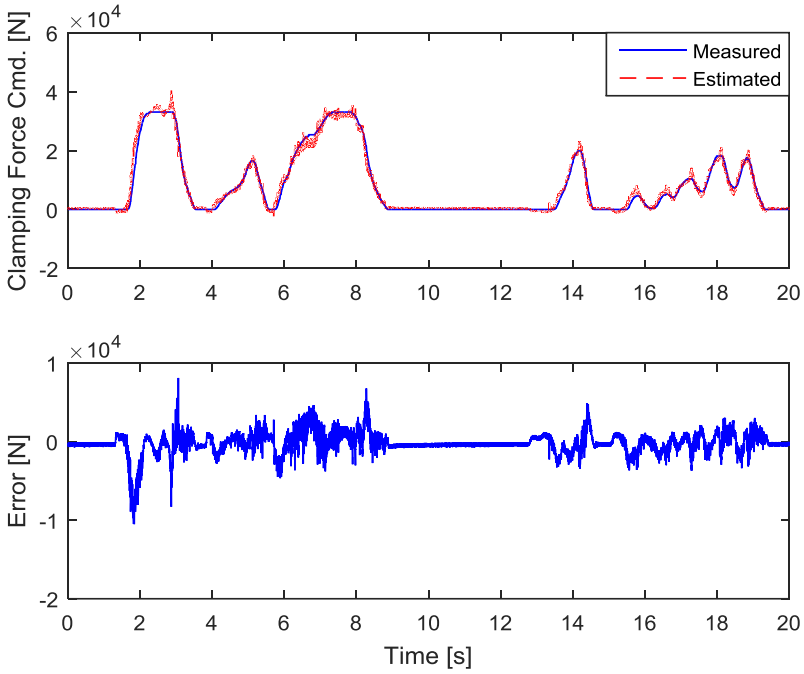

Fig. 3.15. Hybrid GMDH/GA identification results

Table 3.2. Comparison of performances for different identification techniques

Identification Techniques	**RMSE [N]**	**R**
Neural network	3211.8	0.95556
GMDH	1561.8	0.98949
Hybrid GMDH/GA	117.5	0.99223

Table 3.2 shows a numerical comparison of the RMSE and R results from different modeling methods applied to identification of the brake pedal behavior. As indicated in Table 3.2, considering the RMSE and R which are here regarded to be performance indicators, the experimental results clearly demonstrate that the hybrid GMDH/GA outperforms the other identification methods. In the case of the RMSE performance comparison, the hybrid GMDH/GA performed about 92% better than the GMDH and about 96% better than the neural network. Considering the RMSE and R performance, the hybrid GMDH/GA identification may be the best choice because it had the smallest error compared with the other methods. In addition, the hybrid GMDH/GA identification shows good performance in cor-

relation analysis.

3.7 Conclusions

In this chapter, we have presented a hybrid GMDH/GA approach which was successfully used for the modeling and prediction of the brake pedal behavior. In conclusion, the results obtained using the hybrid GMDH/GA were better than those obtained using the other identification methods under random complex braking conditions. The accurate model obtained using the hybrid approach is expected to play an important role in the fault-tolerant control of the BBW systems in the future.

IV. Clamping Force Estimation of Electro-Mechanical Brake Using a Hybrid Genetic Algorithm and Kalman Filter

4.1 Introduction

Recently, X-by-wire (XBW) for vehicle electronic control has been actively studied in the automotive industry. XBW has the effect of improving the design freedom of the vehicle and the fuel efficiency by replacing existing mechanical hydraulics with electrical systems. It was developed to improve actuation response times by replacing the mechanically actuated systems used in conventional vehicles [7]. Furthermore, design and implementation of brake-by-wire (BBW) systems in the XBW has been the focus of researchers and industry experts for decades [12-14]. In previous chapter, Figure 2.2 shows a schematic diagram of the typical BBW systems. The human-machine interface (HMI) in the BBW system is provided by a pedal feel emulator. Such an electronic pedal is equipped with sensors that indicate the level of brake demand required by a driver. The output signals from these sensors are processed by an electronic control unit (ECU) that appropriately controls the actuators. A high level of safety is employed in BBW systems to ensure fault-tolerant operation [20].

The BBW systems approach reduces weight and is more environmentally friendly (due to brake fluid omission) than electro-hydraulic technologies. This scheme uses an electric motor drive coupled to a reduction gear set-up to provide brake control to each wheel. The BBW systems are divided into the electro-hydraulic brake (EHB) which electronically controls the hydraulic brake system using a solenoid valve, and the electro-mechanical brake (EMB) which controls the brakes directly using an electric motor. The EMB types

can be divided into screw-type EMB with screw direct pressurization and electro-wedge brake (EWB) with self-reinforcement features of a wedge structure [33, 34]. The EMB system allows removal of the brake booster and hydraulic hose, so it requires less space, is eco-friendly, and provides faster response time. An electric motor coupled to reduction gearing is the general setup used for the EMB actuator. The motor is typically a three-phase permanent magnet synchronous motor (PMSM) or brushless DC motor for reasons of compactness and enhanced commutation efficiency. Moreover, there are no sparks in this case, unlike when using a brush-type motor. A planetary gear-set connected to a ball-screw are generally the components used in the reduction gearing. The reduction gearing generally consists of a planetary gear-train connected to a ball-screw that can generate clamping force.

To control the EMB caliper clamping force, a clamping force sensor is typically used to close the control loop. A standard motion control architecture (cascaded force, speed, and current control loops), after slight alteration, can be used to control an EMB. Line et al. [8] exchanged the position control loop with a force control loop for EMB control purposes. The control system requires the use of the force sensor (normally an encoder), and the current sensor for a three-phase PMSM.

A clamping force sensor is a relatively high-cost device. The elimination of a clamping force sensor from EMB designs is highly desirable because of the cost, engineering problems, and research challenges involved with its use. Moreover, if a clamping force sensor is placed close to a brake pad, it will then be subjected to severe high temperature that would challenge its mechanically integrity. This situation can be avoided by embedding a clamping force sensor deep within the EMB, (i.e. at the near end of the ball-screw). It has been shown that embedding a sensor in this way leads to hysteresis that is influenced by friction between the clamping force sensor and the pad and disk interface [17]. This hys-

teresis significantly influences the accuracy of the clamping force measurement.

Due to the cost issues and engineering problems involved with using an actual clamping force sensor, an opportunity presents itself for the development of a virtual clamping force sensor. That is, the opportunity here is to accurately estimate the clamping force based on alternative sensor measurements, leading to omission of a clamping force sensor. Accurate clamping force estimation techniques are important for automotive safety-critical systems, and highly dynamic braking situations are known to cause significant inaccuracies in typical clamping force estimation. Also, if the EMB system fails to operate due to a sensor failure, the braking force is lost and the probability of a fatal accident rises sharply.

The focus of this work is to develop a virtual clamping force sensor for sensorless control of automotive BBW systems. Two independent models (dynamic stiffness model and torque balance model) were proposed to estimate clamping force with the help of information from the remaining sensors. Then, a hybrid approach using a Kalman filter and genetic algorithm (GA) was developed to improve clamping force estimation performance. The GA was applied because the distribution of noise is usually unknown, and manual tuning of the Kalman filter using the trial-and-error is very time consuming. A real-coded GA was used to optimize the noise matrices and thereby improve the performance of the Kalman filter. The dynamic stiffness model was used as the state-space system equation, and the torque balance model was used as the measurement equation.

4.2 Related Works

A clamping force estimation algorithm was first studied by Schwarz et al. [17] for

use on an EMB caliper designed for a disk brake. Schwarz et al. [17] proposed a clamping force estimation method using the relationship between the angular displacement of the motor and a clamping force. This method has the advantage that it does not need to consider friction because it utilizes the average torque during the clamping and the releasing; however, this method has errors because nonlinear effects were not considered. Saric et al. [18] proposed another method using the relationship between the angular displacement of the motor and the clamping force in the frequency domain. This method can be adopted in a system that is required to have rapid response characteristics such as anti-lock braking system (ABS). Most recently, Eum et al. [20] proposed a sensorless robust force control for improving the control performance of an EMB applicable for commercial city buses. A cascade control strategy was proposed and a disturbance observer was employed to enhance control robustness against model variation. There have been some previous studies on the estimation techniques used for clamping force in the EMB, but some intrinsic characteristics of the brake unit have not been fully studied.

Sensor fault diagnosis and fault-tolerant control can be found in the literature on PMSM drives [74]. Regarding the motor position estimation method for a PMSM, the literature is concentrated in three main areas. The first group of methods use estimation based on the back-EMF voltage. In voltage model methods, the measured voltage and currents are used to estimate the position of the rotor flux linkage on the basis of the voltage equations of the permanent magnet motor. However, the problem with using the back-EMF technique to estimate position is that at zero speed, the back-EMF approaches zero [75]. The second group of methods uses robust control algorithms, such as sliding mode control techniques. These algorithms are insensitive to parameter variations and disturbances [76]. Therefore, sliding mode control has been presented as a robust estimation method. A negative aspect of the sliding mode control technique is the discontinuous nature of its control action [77].

Finally, the third group of methods consists of techniques based on recursive filter algorithms. These techniques are ideally suited to estimate motor position and speed, and to reject measurement noise [78, 79]. However, tuning of the matrices of the model and the measurement errors is difficult and requires highly skilled operators. Therefore, there have already been approaches to combine a GA with an estimator, e.g. Warwick and Kang [80] used a GA in combination with a recursive least squares algorithm.

4.3 EMB System Modeling

In this section, we briefly summarize the contents of chapter 2 again. Figure 2.3 shows the configuration of the EMB which consists of an electric brake motor, ball-screw, caliper, brake pad, and disk. Figure 4.1 displays a section view of our developed floating type EMB system.

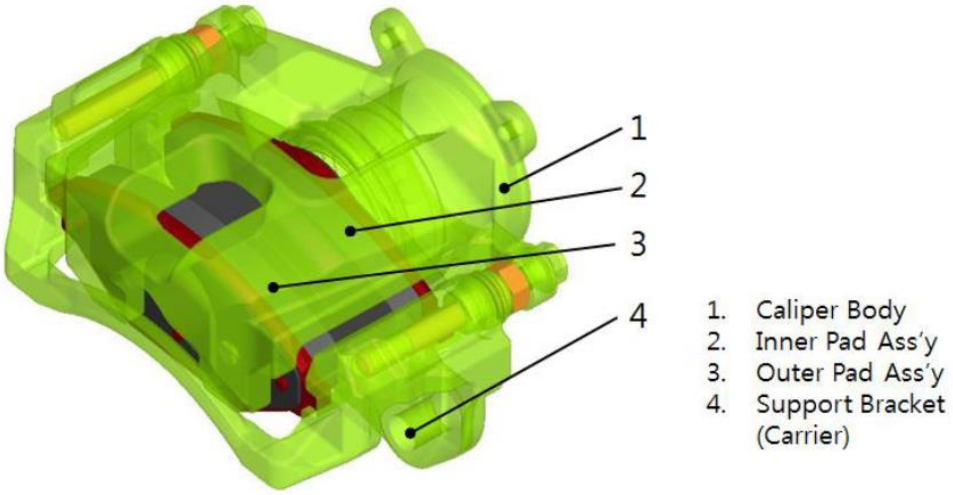

Fig. 4.1. Section view of the developed EMB

4.3.1 Electrical Modeling of the EMB

The EMB system is an electro-mechanical system consisting of an electric motor, caliper, and disk. Therefore, this system requires a complex modeling of both the electric motor (electrical part), and the caliper and disk (mechanical parts).

The motor torque and the motor speed, which correspond to output quantities of the electrical subsystem, are dependent on the controllable magnitude and the adjustable frequency of the inverter output currents, i_a, i_b, and i_c. The three-phase inverter output currents, produced by the pulse-width modulation of the three-phase inverter, are generally dealt with as the dq-axis currents i_d, i_q, and the neutral-axis current i_n in the electronic controller that performs the speed and torque control.

The dq transformation is used for PMSM to transform the reference frame of the voltage, current, and magnetic flux [42].

$$\begin{aligned} v_d &= Ri_d + \frac{d}{dt}\left(L_d i_d\right) - \omega_r \psi_q \\ v_q &= Ri_q + \frac{d}{dt}\left(L_q i_q\right) + \omega_r \psi_d \\ \psi_q &= L_q i_q, \psi_d = L_d i_d + \phi \end{aligned} \tag{4.1}$$

where v_d, v_q is the d-axis and q-axis voltage; i_d, i_q is the d-axis and q-axis stator current; R is the resistance; L_d, L_q is the d-axis and q-axis inductance; ψ_d, ψ_q is the d-axis and q-axis flux linkage; ω_r is the motor synchronous speed (or electrical angular speed); ϕ is the flux linkage due to magnetic rotor.

The electrical motor torque of the PMSM can be expressed as,

$$T_m = \frac{3}{2} P\left[\phi i_q + \left(L_d - L_q\right) i_d i_q\right] \tag{4.2}$$

The maximum torque is generated in the PMSM when the magnetic rotor and the rotating frame are maintained at a right angle with the three-phase current control. In this case, the d-axis current, i_d, is set to zero and the following assumption is made.

$$T_m = \frac{3}{2} P\phi i_q = k_m i_q \tag{4.3}$$

where k_m is a motor torque constant. The relationship between the synchronous speed ω_r and the rotational speed ω_m is as follows.

$$\omega_m \approx \frac{1}{P}\omega_r \tag{4.4}$$

4.3.2 Mechanical Modeling of the EMB

The system used in this study is a method of generating the clamping force needed to push the brake pads. The torque generated by the motor is changed from rotational to translational motion through a ball-screw; then transmitted to the brake pad. The mechanical components of the model are expressed as,

$$T_m = T_l + J\frac{d}{dt}\omega_m + T_f \tag{4.5}$$

where T_l is the load torque, J is the moment of inertia, ω_m is the motor angular speed,

T_f is the resistance torque due to friction and viscosity.

The load torque is directly related to the clamping force between the brake pad and rotor. The resistance torque is mainly from viscous friction torque in the ball-screw.

$$T_l = \frac{p_s}{2\pi n_g \eta} F_{cl} = \gamma F_{cl} \tag{4.6}$$

where F_{cl} is the clamping force, p_s is the screw pitch, n_g is the gear ratio, η is the screw efficiency, and γ is the gear-train gain.

4.3.3 Nonlinear Characteristics in the EMB

The dominant nonlinearities to consider in the EMB system are force ripple and friction. These are caused by the electromagnetic structure of the motor, the mechanical structure from which torque generated by the motor is converted to the clamping force through the caliper and other imperfect physical factors.

Force ripple is caused by cogging force and reluctance force. The cogging force occurs as a result of mutual attraction between the rotor magnet and the slot of the stator, which occurs even when no current flows through the windings and appears as a periodic relationship to the position of the stator relative to the magnet. The reluctance force is caused by the change in the self-inductance of the winding to the relative position between the magnet and the stator. In particular, the force ripple appears to be large at low speed or low load. In order to solve this problem, it is necessary to design the motor with consideration of the electromagnetic structure to minimize the force ripple, and to provide a control technique for ripple rejection.

Friction is the most nonlinear phenomenon in the entire system due to the nonlinear characteristics of all mechanical systems. This phenomenon is also seen in the EMB system, which causes errors and performance degradation.

In previous studies, several models have been proposed to explain the phenomenon caused by friction. In general, friction acts in the direction opposite the motion, and the friction model is expressed in the form of a function of velocity. A typical friction torque model can be represented by a combination of Coulomb friction, viscous friction, and Stribeck friction torque [31].

$$T_f = \left[T_c + (T_s - T_c) e^{-|\omega_m/\omega_s|^2} \right] \mathrm{sgn}(\omega_m) + B_v \omega_m \tag{4.7}$$

where T_c is the Coulomb friction torque, T_s is the stiction friction torque, ω_s is the Stribeck velocity, and B_v is the coefficient of viscous friction.

4.4 Estimation of the EMB Clamping Force

4.4.1 Dynamic Considerations

Figure 4.2 shows the clamping force versus motor position where the latter is varied in a uniform random manner. The uniform random means that all numbers within a specified range can lead to the same chance of occurring. It is apparent from Figure 4.2 that there is significant dynamics in the system, and that the use of a characteristic curve to estimate the clamping force has limitations for highly dynamic cases. The clamping force was ele-

vated during apply and reduced during the release. It was tested in total 4 times of applying and releasing actions. The cause of this dynamic will be described and modeled in the following section.

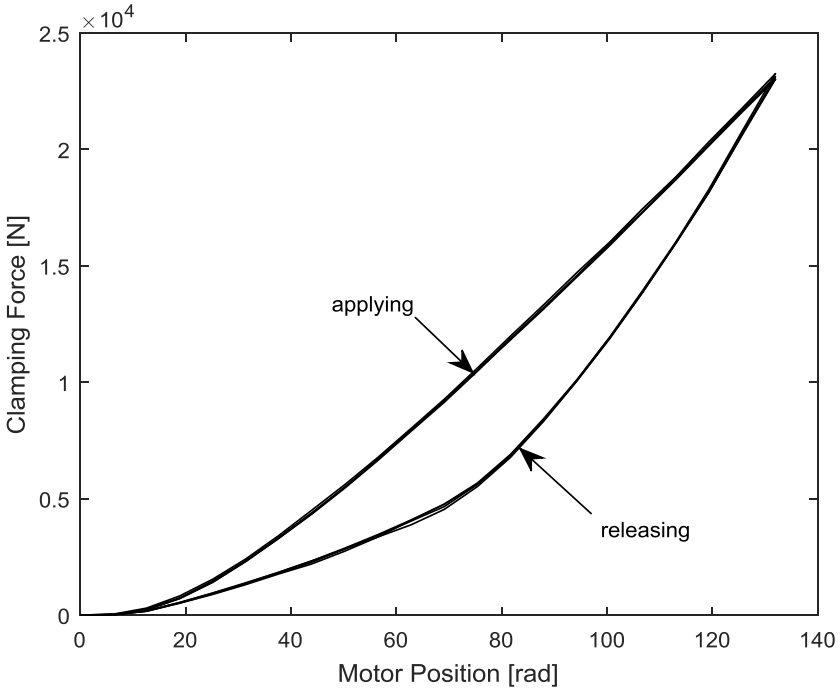

Fig. 4.2. Characteristic curve for the EMB

4.4.2 Dynamic Stiffness and Torque Balance Modeling

As shown in section 3, to determine an induced clamping force in an EMB caliper using motor current information, the model can be solved as follows:

$$k_m i_q = T_l + J\frac{d^2\theta_m}{dt^2} + T_f$$
$$F_{cl} = \frac{k_m i_q - J\frac{d^2\theta_m}{dt^2} - T_f}{\gamma} \tag{4.8}$$

Application torque T_l is linearly proportional to the clamping force F_{cl} with reduction gearing gain γ, which is determined using the specifications from the gear-train and ball-screw. The inertial torque is linearly proportional to the motor angular acceleration $d^2\theta_m/dt^2$ with a lumped inertia gain J that involves both rotational and translational motions.

Eq. (4.8) shows that the frictional torque T_f term is undefined, this is because as Olsson et al. [43] explained, deriving an accurate friction model from first principles is simply not possible due to the random nature of friction. To improve accuracy, general friction models should be used in accordance with compensation for friction phenomena that occur in a particular system. Friction models of any sort tend to be avoided in trying to estimate the clamping force in an EMB caliper because of issues related to accounting for wear in the reduction gearing.

Employment of an applying and releasing action technique avoids the need for using a friction model, which is explained in more detail as follows [81, 82]. At both these instants the application of Eq. (4.8) yields:

$$\begin{aligned} T_{m,cl} &= \gamma F_{cl} + J\frac{d^2\theta_{m,cl}}{dt^2} + T_f \\ T_{m,rl} &= \gamma F_{cl} + J\frac{d^2\theta_{m,rl}}{dt^2} - T_f \end{aligned} \tag{4.9}$$

where $T_{m,cl}$ and $T_{m,rl}$ indicate applying and releasing torque, respectively. The friction terms in Eq. (4.9) have approximately the same magnitudes but opposite signs due to the change in the course of motor travel. Adding Eq. (4.9) cancels out the friction terms, and after some manipulation the following equation to estimate clamping force F_{cl} can be

found:

$$F_{cl} = \frac{T_{m,cl} + T_{m,rl} - J\dfrac{d^2\left(\theta_{m,cl} + \theta_{m,rl}\right)}{dt^2}}{2\gamma} \tag{4.10}$$

In general, the main problem with this method for clamping force estimation is the limitation for high speed applications. It is very difficult to collect the applying and releasing actions with the same motor angle information at high speed. A means to cope with these problems was first proposed by Schwarz et al. [17], who put forward the use of a caliper characteristic curve to provide feedback control of the applied clamping force. In the instants where Eq. (4.10) can be applied, it is used to adapt the parameter variations in the characteristic curve associated with pad wear and thermally dependent stiffness changes.

Saric et al. [18] developed a dynamic stiffness model to handle such viscoelastic effects. Consider a first order transfer function expressed by the following equation:

$$G(s) = \frac{F_{cl}(s)}{\theta_m(s)} = \frac{K_t}{\tau s + 1} \tag{4.11}$$

where θ_m and F_{cl} denote the motor position and estimated clamping force in s-domain, respectively. The gain K_t and time constant τ are the parameters to be determined. Converting Eq. (4.11) into time-domain yields:

$$F_{cl} = K_t\theta_m - \tau\frac{dF_{cl}}{dt} \tag{4.12}$$

When the electric motor is at low speed $dF_{cl}/dt \approx 0$, therefore the clamping force will nearly be linearly proportional to the motor position. However, as shown in Figure 4.2, a characteristic curve for an EMB is non-linear and can be accurately described by a third-order polynomial. This non-linearity, at the very least, can be attributed to variation in stiffness exhibited by the brake pads and the caliper bridge [83]. Based on this, a more accurate variation of Eq. (4.12) is as follows:

$$F_{cl} = \Lambda_2 \theta_m^3 + \Lambda_1 \theta_m^2 + \Lambda_0 \theta_m - \tau \frac{dF_{cl}}{dt} \tag{4.13}$$

where Λ_2, Λ_1, and Λ_0 are stiffness parameters. The discrete-time notation of Eq. (4.13) is more practical for use in a digital processing system and is expressed in a simplified form as follows:

$$F_{cl}(k) = \alpha_3 \theta_m^3(k) + \alpha_2 \theta_m^2(k) + \alpha_1 \theta_m(k) + \alpha_0 F_{cl}(k-1) \tag{4.14}$$

where α_3, α_2, α_1, and α_0 are experimentally determined constants. Because high speed measurement was used for parameter tuning in Eq. (4.14) such situations are weighted more heavily with regards to accuracy. This is a desired outcome because it allows performance for high deceleration safety-critical braking situations to be optimized.

The generalized discrete-time model based on the torque balance approach will now be described. A simplified friction model is as follows [43]:

$$T_f = \left(\mu_g F_{cl} + C\right) \operatorname{sgn}\left(\frac{d\theta_m}{dt}\right) \tag{4.15}$$

where μ_g and C are the reduction gearing coefficient of kinetic Coulomb friction and kinetic friction offset respectively. The kinetic friction offset is required to take into account frictional resistance prior to inducing a clamp. The sign function $\mathrm{sgn}(\cdot)$ (1 for positive and -1 for negative arguments) is included to model the friction sign change that occurs between applying and releasing actions. It should be noted that stiction is not included in the friction model. This is because this paper is concerned only with estimating the clamping force for dynamic braking scenarios.

To calculate clamping force using a torque balance model approach, it is necessary that the friction model parameters be updated at timely intervals. A discrete-time form for practical use in clamping force is as follows:

$$T_m(k) = \gamma F_{cl}(k) + \frac{J}{\Delta t^2}\left(\theta_m(k) - 2\theta_m(k-1) + \theta_m(k-2)\right) + \left(\mu_g F_{cl}(k) + C\right)\mathrm{sgn}\left(\theta_m(k) - \theta_m(k-1)\right) \quad (4.16)$$

where Δt is the sampling time.

After some algebraic manipulation of Eq. (4.16), the result is shown below in discrete-time notation:

$$F_{cl}(k) = \frac{T_m(k) - \frac{J}{\Delta t^2}\left(\theta_m(k) - 2\theta_m(k-1) + \theta_m(k-2)\right) - C\,\mathrm{sgn}\left(\theta_m(k) - \theta_m(k-1)\right)}{\gamma + \mu_g\,\mathrm{sgn}\left(\theta_m(k) - \theta_m(k-1)\right)} \quad (4.17)$$

The following section details how we setup the novel Kalman filter optimized by GA for tracking EMB clamping force obtained from Eq. (4.14) and (4.17).

4.5 Design of a Hybrid Genetic Algorithm and Kalman Filter to Combine the Dynamic Stiffness Model and Torque Balance Model

4.5.1 Combining the Dynamic Stiffness Model and Torque Balance Model Using a Kalman Filter

In the previous chapter, we introduced the dynamic stiffness model and the torque balance model. In this chapter, we design a Kalman filter suitable for the EMB clamping force virtual sensor and fuse and track both models. A Kalman filter is a linear, recursive, and optimal estimator and is widely implemented in control systems to give improved system state estimates [84]. Figure 4.3 shows a block diagram representation of a Kalman filter in a control system. By using recursive calculations, the Kalman filter is capable of estimating the state of a linear dynamic system from a series of noisy measurements (Gaussian noise). The Kalman filter uses system dynamics as well as other measurement sources to estimate states. The noises that affect both of the kinds of estimates received by the Kalman filter (see Figure 4.3), are required to be uncorrelated.

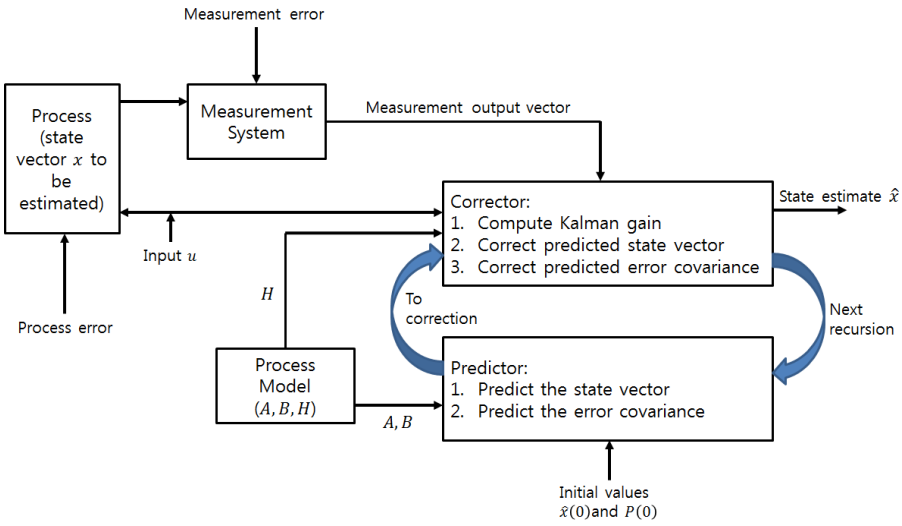

Fig. 4.3. Computational scheme of a discrete Kalman filter

The Kalman filter is able to estimate unknown variables of a dynamic system using the following information [85]:

1) A linear model of the dynamic system including statistics (covariance matrix Q) of the random disturbances that enter the system (including random model error).

2) A linear relationship between the measurable output variables of the dynamic system and the variables to be estimated. This relationship may be represented by an output matrix (i.e., measurement matrix) H, and also includes random noise (i.e., random measurement error) with covariance matrix R.

3) Output measurements.

The Kalman filter uses a predictor-corrector approach, which consists of the following two steps:

1) Predict the unknown variables and the associated error covariance matrix. This is an a priori estimate. This predictor step uses the process model and the covariance matrix of the input disturbances (including the model error).

2) Correct the predicted variables and the associated error covariance matrix. This is an a posteriori estimate. This corrector step uses the output relationship (measurement matrix) and the covariance matrix of the measurement noise.

The derivation of the Kalman filter algorithm is as follows. A discrete state-space representation of a linear dynamic system with noises may be written in the following form:

$$\begin{aligned} x(k) &= Ax(k-1) + Bu(k) + w(k-1) \\ z(k) &= Hx(k) + v(k) \end{aligned} \tag{4.18}$$

where x is the system state vector, u is the control inputs, w is the process error vector,

z is the measurement vector, v is the measurement error vector, K is the Kalman filter gain, A is the transition matrix, B is the control input matrix, and H is the measurement matrix.

It is assumed that the transition matrix and control input matrix are not time-varying. The discrete-time notation, $k|k-1$, indicates that the estimate at k was determined given knowledge at $k-1$. The linear estimator and filter gain are defined as follows:

$$\hat{x}(k|k) = \hat{x}(k|k-1) + K(k)\left(z(k) - H\hat{x}(k|k-1)\right) \tag{4.19}$$

$$K(k) = P(k|k-1)H^T(k)\left(H(k)P(k|k-1)H^T(k) + R\right)^{-1} \tag{4.20}$$

where P is the covariance matrix of state estimates, and R is the measurement error covariance matrix.

The matrices $P(k|k-1)$ and $P(k|k)$ for a Kalman filter are given below as:

$$P(k|k-1) = A(k)P(k-1|k-1)A(k)^T + Q \tag{4.21}$$

$$P(k|k) = \left(I - K(k)H(k)\right)P(k|k-1) \tag{4.22}$$

where Q is the process error covariance matrix, and I is the identity matrix.

It should be noted that the process error covariance Q and measurement error covariance R matrices may be time-variant, however, here, we assume them to be constant. A Kalman filter of any type involves the recursive application of prediction and filtering cycles. Many researchers have given complete derivations of the Kalman filter algorithm [86-89].

To employ a Kalman filter for the EMB clamping force estimation, we first used Eq. (4.14) as our state-space system equation. The constant α_0 from Eq. (4.14) is taken to be equal to $A(k)$. The clamping force in Eq. (4.14) is non-linearly proportional to the motor position input data. This non-linearity does not require the use of an extended Kalman filter (EKF) because it is not state dependent. To integrate this non-linearity within the Kalman filter algorithms we apply the following equality:

$$\begin{aligned} A(k)x(k-1) &= \alpha_0 F_{cl}(k-1), \\ B(k)u(k) &= \alpha_3\theta_m^3(k) + \alpha_2\theta_m^2(k) + \alpha_1\theta_m(k) \end{aligned} \tag{4.23}$$

where $\hat{x}$ is taken to be $\hat{F}_{cl}$. The a priori estimate of the state $\hat{F}_{cl}(k|k-1)$ is taken to be directly equal to $\hat{z}(k|k-1)$. The measurement equation is as follows:

$$\begin{aligned} \hat{z}(k\,|\,k-1) &= \hat{F}_{cl}(k\,|\,k-1), \\ z(k) &= F_{cl}(k) + v(k) \end{aligned} \tag{4.24}$$

For this situation, the matrix $H(k)$ is taken to have a constant unit value. In Eq. (4.24), the measured data is substituted into the calculated clamping force of Eq. (4.17). The two models are combined using the Kalman filter to give an optimized estimate of clamping force. Figure 4.4 shows a block diagram of the Kalman filter applied to the EMB system.

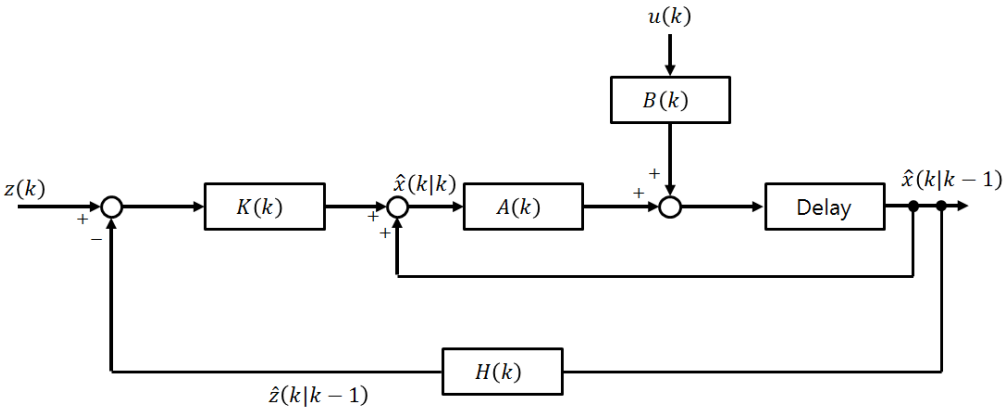

Fig. 4.4. Block diagram of the Kalman filter for the EMB system

4.5.2 Optimizing the Noise Matrices of a Hybrid Genetic Algorithm and Kalman Filter

Since we cannot know Q and R matrices in a real vehicle environment, we propose a method to improve the EMB clamping force estimation performance by applying optimization technique to the Kalman filter. The GA, introduced by John Holland, is a method based on biological evolution [90]. Essentially, the GA is a guided random search technique, which follows a scheme of random selection, evaluation and evolution, and a good research summary may be found in [26].

The GA has a powerful encoding mechanism that enables the representation of a solution vector as either a binary string or real-coded. In order to find the best matrices Q, and R for the Kalman filter, a real-coded GA was employed. The real-coded GA has many advantages for optimization of numerical function over binary encoding. Efficiency of the real-coded GA is increased because there is no need to convert chromosomes to phenotypes before each fitness evaluation; less memory is required and; there is no loss in precision from the conversion between binary and real values. The procedure for making the real-coded is outlined as follows [91]:

1) Population Representation: The covariance matrices Q, and R are coded into a long

real-coded string, chromosome.

2) Initial Generation: The process begins by randomly generating an initial population of long real-coded strings.

3) Fitness Evaluation: In the current generation, each of the strings is decoded back to the corresponding diagonal elements of the two matrices. Then, these diagonal elements from each string are separately sent to the Kalman filter of the EMB system to yield an objective function (which is the mean squared error of the predicted clamping force). Finally, these strings are ranked according to the value of the objective function by a linear ranking method.

4) Reproduction: Reproduction is a process in which parent structures are selected to form new offspring (children). For this, the stochastic universal sampling method was employed.

5) Crossover: The single-point recombination method is used to exchange information between two chromosomes.

6) Mutation: A Breeder GA is used to implement the mutation operator for the real-coded GA, which uses a nonlinear term for the distribution of the range of mutation applied to the gene values. This mutation algorithm is able to generate most points in a hypercube defined by the variables of the individual and range of the mutation. By biasing mutation towards smaller changes in gene values, the mutation can be used in conjunction with recombination as a foreground search process.

7) Replace: Place new offspring in the old population to create a new population and use the newly generated population for the next run of the algorithm.

8) Iteration: The real-coded GA runs iteratively repeating processes 3) to 7) until a population convergence condition is met, or the given maximum number of iterations is reached.

The GA calculation procedure is summarized in Figure 4.5.

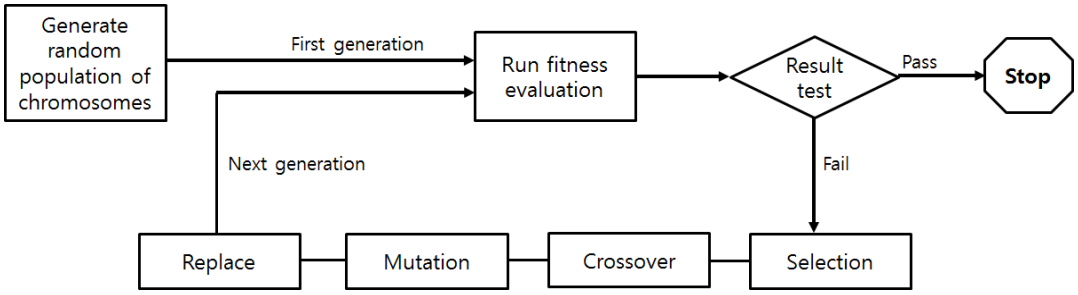

Fig. 4.5. GA calculation process

With the Kalman filter optimized by GA concept to track the clamping force in the EMB system defined, the next section briefly describes the test bench developed to obtain necessary the data for analysis.

4.6 Experimental Setup and Results

4.6.1 Experimental Setup

Our test bench was setup for use on the newly developed EMB caliper. Figure 4.6 shows the developed systems. The electric motor is of the PMSM-type maxon EC-4 pole 30 motor, with ratings of 200 W and 15,000 rpm and ensures that maximum clamping forces can be achieved. To interface with the motor and ECU devices, the CAN and FlexRay net-works were utilized. The PC provides a real-time operating system that was implemented to control the motor position. The electric motor is controlled by cascaded PI controller with the standard motion control architecture; force, speed, and current control loops. The PC has an Intel Core CPU 1.5 GHz and RAM 8 GHz. To measure the motor position, encoder output is taken from the coupled the servo-motor. The resolution of this encoder output provides 1,000 counts per turn. A clamping force sensor is placed in between the brake

pads to measure the actual force induced by the brake pads. The sensor data was collected using the DEWETRON monitoring system. The monitoring system updates in-vehicle information received from each ECU via CAN and overall EMB status information in real-time. Figure 4.7 shows the actual clamping force signal measured for 32 seconds for the stepwise dynamic braking. The clamping force sensor data was gathered at 0.2 ms sample intervals. Therefore, total acquired data are 160,000 samples.

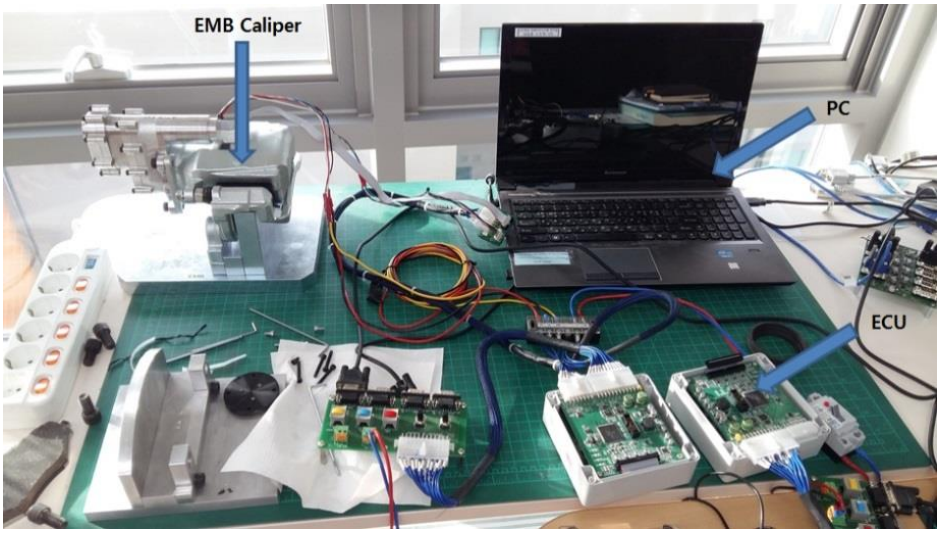

Fig. 4.6. Test bench with the EMB

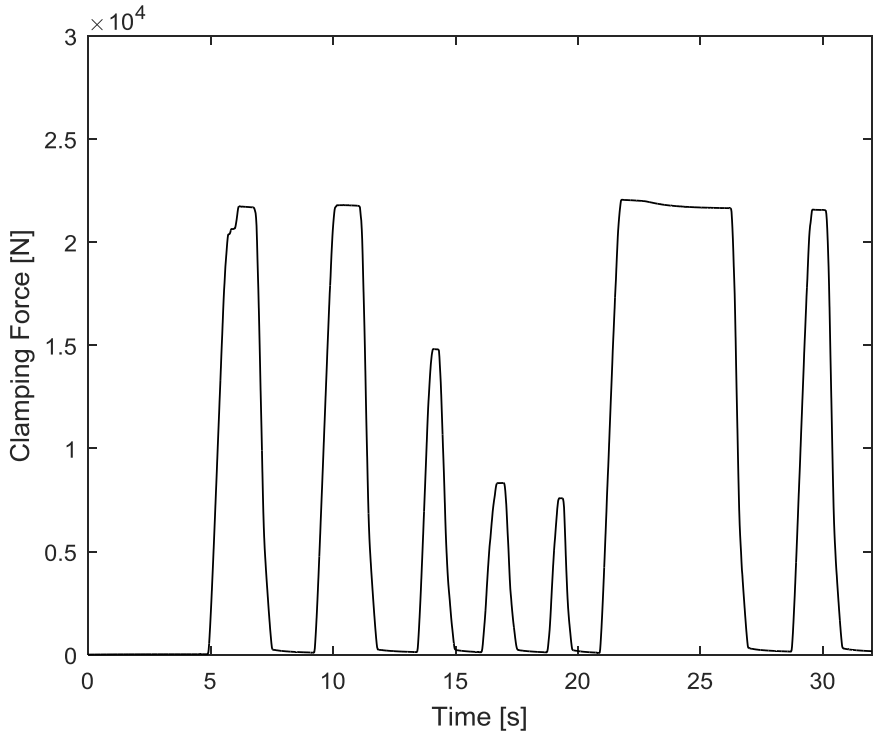

Fig. 4.7. Actual clamping force for stepwise dynamic braking

4.6.2 Comparison of Results and Discussions

The Kalman filter used for tracking the clamping force was applied to the two model's data. We used constant process error variance of 1 and measurement noise variance of 1 to initialize the error variance. Then, the GA was implemented on the PC. To optimize the noise matrices of the Kalman filter for the EMB system, the parameters of the GA were set as follows:

1) Initial population size: 40,

2) Maximum number of generations: 20,

3) Probability of crossover: 0.9,

4) Mutation probability: 0.01,

5) Initial range of real-coded strings: [0.0001; 0.1].

Figure 4.8 shows a gradient convergence process of the real-coded GA. At the 20th generation, the best mean squared error (MSE) of the predicted clamping force has decreased to 8649.778 with the optimized matrices Q, and R.

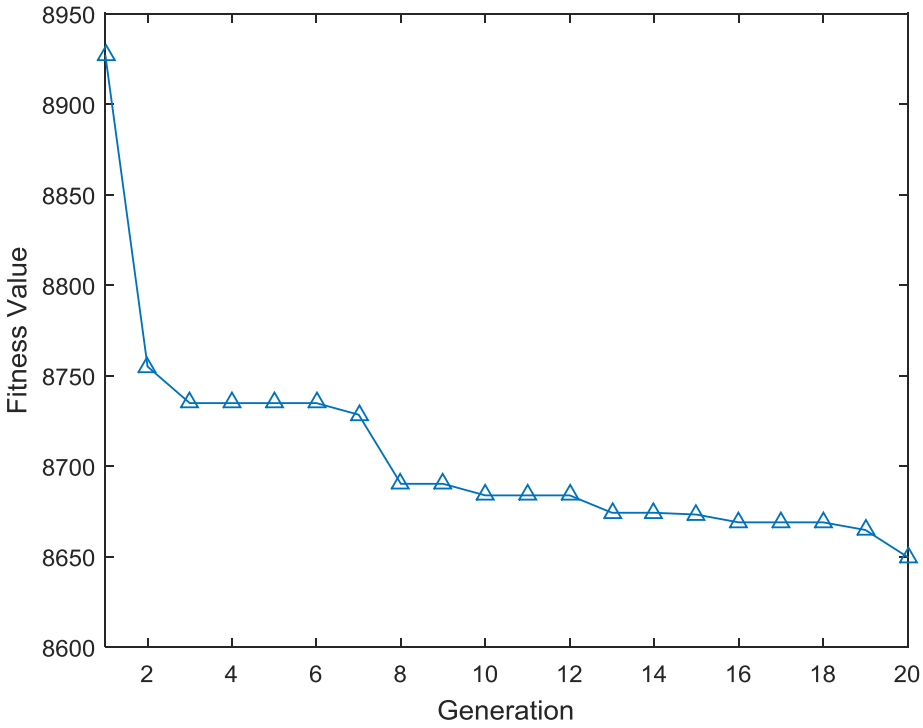

Fig. 4.8. Iteration of GA

Figure 4.9 shows the estimation performance of the proposed method to track the clamping force in the EMB system for various clamping force. We used the root mean squared error (RMSE) between actual and estimated values as performance indicators. During total 32 seconds, RMSE of the dynamic stiffness model and torque balance model was 404.670 N and 413.773 N, respectively. The RMSE of the hybrid GA/Kalman filter was 324.796 N. This is approximately 21.44% improvement on the RMSE of the Kalman filter alone of 413.449 N for total 32 seconds. Therefore, we have demonstrated that the use of

hybrid GA/Kalman filter which has a recursive aspect, improves the RMSE performance of the clamping force estimation. In order to verify the validity of the experiment, the simulation was performed using the EMB model developed by MATLAB/Simulink. The results are shown in Figure 4.10.

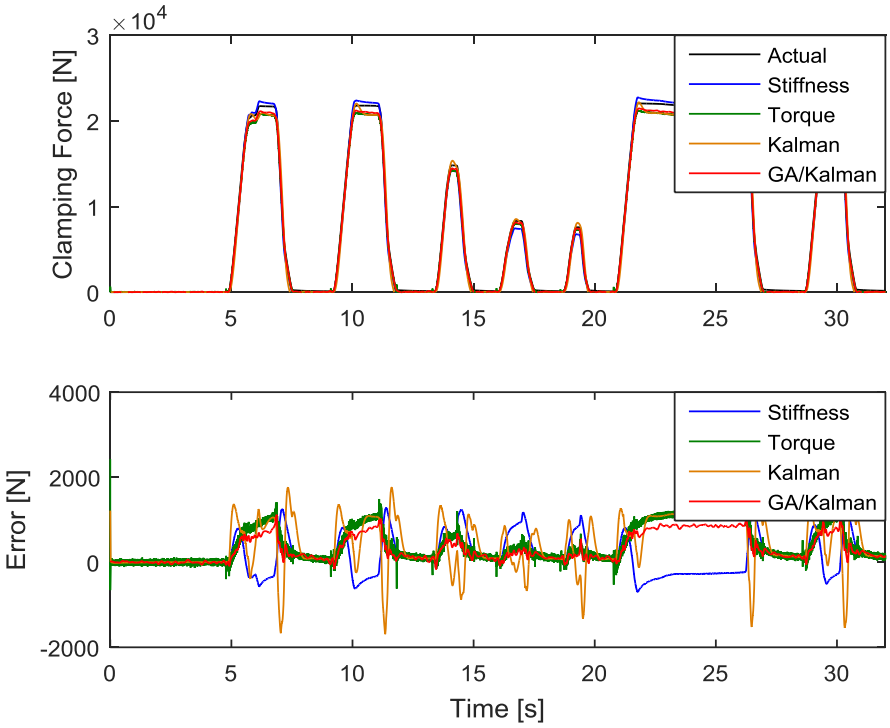

Fig. 4.9. Experimental results of clamping force estimation

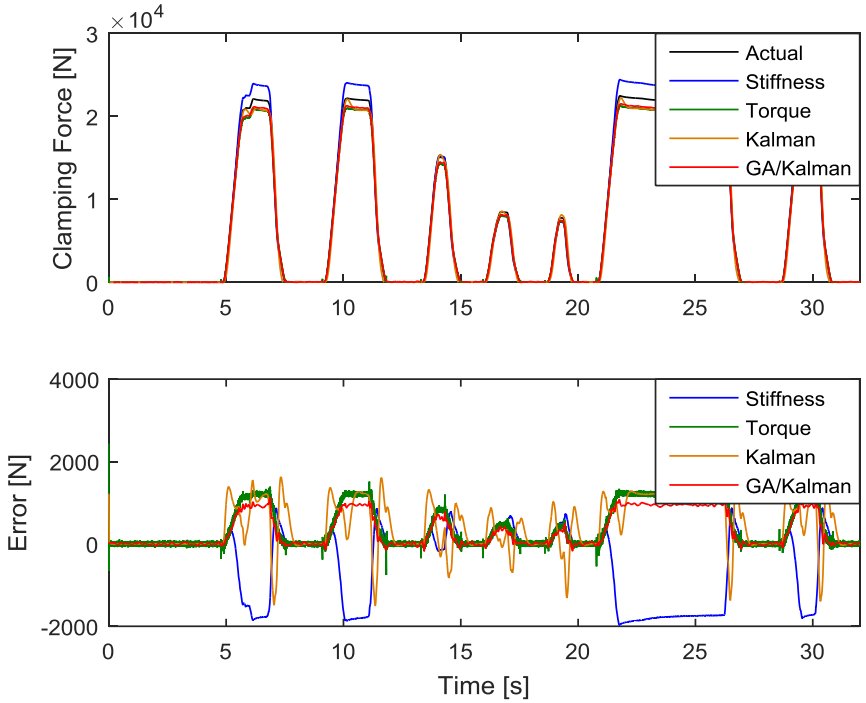

Fig. 4.10. Simulation results of clamping force estimation

The RMSE performances of each estimation techniques are summarized in the Table 4.1.

Table 4.1. Comparison of RMSE performances for different estimation techniques

Estimation techniques	RMSE [N] (Experiment)	RMSE [N] (Simulation)
Dynamic stiffness model	404.670	391.325
Torque balance model	413.773	420.916
Kalman filter	413.449	420.653
Hybrid GA/Kalman filter	324.796	330.904

We refer to Ref. [81] for selecting the criteria of estimation accuracy. The author's goal is to have a smaller RMSE than a clamping force of 390 N at 0.03 g of vehicle longitudinal deceleration in the braking range from 0 to 12 kN and sampling intervals of 1 ms. This is a target value set on the assumption that a deceleration of about 0.03 g occurs when a clamping force of 390 N is generated at four wheels during braking of the vehicle. It can

be confirmed that the estimation accuracy is satisfactory since the RMSE result of the hybrid GA/Kalman filter is smaller than the target value of 390 N. Especially, since our developed EMB system has more than twice the braking range than the system of Ref. [81], the estimation accuracy seems to be satisfactory. This estimation performance shows that its adaptation for sensorless and fault-tolerant control is possible.

The advantage of the GA is that a large range of parameters can easily be covered without exact a priori knowledge of the actual parameters. One disadvantage of the proposed approach is the demand for high computation power. This is not a problem, while doing the calculation offline. For online estimation, however, the calculation has to be done in less than real-time, thus requiring several parallel processors, which would increase the cost of implementation. Therefore, the practical engineers will need to make appropriate application of the GA for the EMB system.

4.7 Conclusions

In this chapter, we proposed a cost and design effective solution for an automotive EMB actuator in BBW systems. The objective of making a virtual clamping force sensor in the EMB system is strongly encouraged by the results. A dynamic stiffness model was used to estimate the clamping force that relied on output from an encoder. Based on a torque balance approach, a second model was used to estimate the clamping force that relied on the use of the motor current sensor and encoder. The outputs from the two independent models were combined using a hybrid GA/Kalman filter to give accurately track the actual clamping force. The newly developed estimator was shown via experimental verification to be able to handle highly dynamic braking situations. Real-coded GA was found to be a power

technique for optimizing the Kalman filter as applied to the EMB system. Based on a real-coded GA, the optimization procedure enables the noise matrices, on which the Kalman filter performance critically depends, to be properly selected. The experimental results demonstrated that the Kalman filter optimized by GA has good noise rejection and that its performance is less sensitive during the dynamic braking. With continued development, the possible cost savings inherent in making an accurate virtual clamping force sensor could be accomplished in the EMB implementations. However, the clamping force estimator validations were not performed yet on a rotating disk in the real car. The significance of this issue should be investigated in future work.

V. Conclusions and Future Works

The EMBs are the brake systems that replace existing hydraulic braking systems with eco-friendly and future-oriented technologies and are key technologies for hybrid vehicles. In this thesis, mathematical modeling and the controller for the EMB system were designed and implemented using MATLAB/Simulink. In order to simulate the rotational motion of motor and reducer, a friction model including Coulomb, viscous, and static friction model was used and the LuGre model was used to simulate the friction generated from the screw by the clamping force. The EMB controller is a cascaded PI type, and the clamping force controller, speed controller, and current controller are located in order from the outside to the inside.

Then, we proposed a novel identification and estimation method for sensorless control of an EMB system used as a braking actuator in the BBW systems. In the existing literature, there was insufficient study on sensorless and fault-tolerant control of the EMB system. In this study, we proposed the system identification and estimation based on hybrid soft computing, and suggested a method to control the braking force using the estimated value even in the case of sensor failure. In the EMB system, the electronic pedal sensor system including the ECU and the clamping force sensor are very important factors in terms of safety. In the identification study of the electronic pedal system, the performance is clearly improved by the hybrid method relative to the conventional methods. The clamping force estimation study employed combined model based on a dynamic stiffness model and a torque balance model considering the hysteresis during applying and releasing. Also, the Kalman filter algorithm optimized by GA improves the estimation performance. Considerable amounts of experimental data have been presented in this thesis and this data can pro-

vide material support for continued future research in the emerging technology.

In order to improve the existing methods to estimate the clamping force, further research is required. The thermal expansion of the disk was not modeled. An empirically based model of the disk thermal expansion with temperature could be developed in future work. In addition, the clamping force estimator validations were not performed on a rotating disk in a real car. The significance of these issues should be investigated in future work.

As such, the EMB is an eco-friendly and future-oriented technology, and R&D is indispensable for regenerative braking systems in green cars such as hybrid vehicles, electric vehicles, and fuel cell vehicles as well as for improving the performance of existing vehicle brake systems. In addition to the above-mentioned estimation techniques, research on ABS control logic in vehicles with the EMB and efficient regenerative braking studies in hybrid vehicles should be continued in the future.

References

[1] Kelling, N., and Leteinturier, P., "X-by-Wire: Opportunities, Challenges and Trends," *SAE Tech. Paper 2003-01-0113*, 2003.

[2] Savaresi, S. M., and Tanelli, M., *Active Braking Control Systems Design for Vehicles*, Springer, 2010.

[3] Sho, M., Park, K., Park, M., and Kim. M., "Development of a Fail-Safe Control Strategy for Electro-Mechanical Brake System," *SAE Tech. Paper 2013-01-0055*, 2013.

[4] 김대성 외, 차세대 지능형 샤시 시스템 기술 연구, 부품소재혁신연구회 최종보고서, 지식경제부/한국산업기술진흥원, 2010,

[5] "Strategic Analysis of European Markets for X-by-wire Systems," *Frost & Sullivan*, 2007.

[6] Shim, T., Chang, S., and Lee, S., "Investigation of Sliding-Surface Design on the Performance of Sliding Mode Controller in Antilock Braking Systems," *IEEE Trans. on Vehicular Technology*, Vol. 57, No. 2, pp. 747-759, Mar. 2008.

[7] Schwarz, R., Isermann, R., Böhm, J., Nell, J., and Rieth, P., "Modeling and Con-

trol of an Electromechanical Disk Brake," *SAE Tech. Paper 980600*, 1998.

[8] Line, C., Manzie, C., and Good, M., "Control of an Electromechanical Brake for Automotive Brake-By-Wire Systems with an Adapted Motion Control Architecture," *SAE Tech. Paper 2004-01-2050*, 2004.

[9] Line, C., Manzie, C., and Good, M., "Electromechanical Brake Modeling and Control: From PI to MPC," *IEEE Trans. on Control Systems Technology*, Vol. 16, No. 3, pp. 446-457, May, 2008.

[10] Haggag, S. A., and Abidou, D., "An Approach to Vehicle Brake-By-Wire Optimal Control Tracking Strategy," *SAE Tech. Paper 2013-01-0686*, 2013.

[11] 김수병, 전재한, 천재승, "브레이크 시스템의 미래," 오토저널, 26(5), pp. 3-10, 2004 년 10 월.

[12] Hwang, W., Han, K., and Huh, K., "Fault Detection and Diagnosis of the Electro-Mechanical Brake Based on Observer and Parity Space," *International Journal of Automotive Technology*, Vol. 13, No. 5, pp. 845-851, Mar. 2012.

[13] Ki, Y. H., and Ahn, H. S., "Fault-Tolerant Control of EMB Systems," *SAE Tech. Paper 2012-01-1795*, 2012.

[14] Hwang, W., and Huh, K., "Fault Detection and Estimation for Electromechani-

cal Brake Systems Using Parity Space Approach," *Journal of Dynamic Systems, Measurement, and Control*, 137(1), Aug. 2014.

[15] Blanke, M., Kinnaert, M., Lunze, J. and Staroswiecki, M., *Diagnosis and Fault-Tolerant Control*, Springer, 2006.

[16] Isermann, R., *Fault-Diagnosis Systems: An Introduction from Fault Detection to Fault Tolerance*, Springer, 2006.

[17] Schwarz, R., Isermann, R., Böhm, J., Nell, J., and Rieth, P., "Clamping Force Estimation for a Brake-By-Wire Actuator," *SAE Tech. Paper 1999-01-0482*, 1999.

[18] Saric, S., and Bab-Hadiashar, A., "Clamp Force Estimation for a Brake-By-Wire System: A Sensor Fusion Approach," *IEEE Trans. on Vehicular Technology*, Vol. 57, No. 2, pp. 778-786, Mar. 2008.

[19] Hoseinnezhad, R., "Position Sensing in Brake-By-Wire Callipers Using Resolvers," *IEEE Trans. on Vehicular Technology*, Vol. 55, No. 3, pp. 924-932, May 2006.

[20] Eum, S., Choi, J., Park, S. S., Yoo, C., and Nam, K., "Robust Clamping Force Control of an Electro-Mechanical Brake System for Application to Commercial City Buses," *Energies*, 10(2), Feb. 2017.

[21] Petersen, I., "Wheel Slip Control in ABS Brakes Using Gain Scheduled Optimal Control with Constraints," *Ph. D. Thesis*, Norwegian University of Science and Technology, Trondheim, Norway, 2003.

[22] Zadeh, L. A., "A Critical View of Our Research in Automatic Control," *IRE Trans. on Automatic Controls*, AC-7, 74, 1962.

[23] Zadeh, L. A., "The Evolution of Systems Analysis and Control: A Personal Perspective," *IEEE Control Systems*, Vol. 16, No. 3, pp. 95-98, Jun. 1996.

[24] Zadeh, L. A., "Fuzzy Logic, Neural Networks, and Soft Computing," *Communication of the ACM*, Vol. 37, No. 3, pp. 77-84, Mar. 1994.

[25] Dote, Y., and Ovaska, S., "Industrial Applications of Soft Computing: A Review," *Proceedings of the IEEE*, Vol. 89, No. 9, pp. 1243-1265, Sep. 2001.

[26] Seising, R., and Tabacchi, M. E., "A Very Brief History of Soft Computing: Fuzzy Sets, Artificial Neural Networks and Evolutionary Computation," *IFSA World Congress and NAFIPS Annual Meeting*, pp. 739-744, Jun. 2013.

[27] Oh, S. K., Pedrycz, W., and Ahn, T. C., "Self-Organizing Neural Networks with Fuzzy Polynomial Neurons," *Applied Soft Computing*, 2(1), pp. 1-10, Aug. 2002.

[28] Onwubolu, G. C., *Hybrid Self-Organizing Modeling Systems*, Springer, 2009.

[29] Farlow, S., "The GMDH algorithm of Ivakhnenko," *The American Statistician*, 35(4), pp. 210-215, Nov. 1981.

[30] Farlow, S., *Self-Organizing Methods in Modeling: GMDH Type Algorithms*, CRC Press, 1984.

[31] Jo, C., Hwang, S., and Kim, H., "Clamping Force Control for Electromechanical Brake," *IEEE Trans. on Vehicular Technology*, Vol. 59, No. 7, pp. 3205-3212, Sep. 2010.

[32] Ki, Y. H., Lee K. J., Cheon, J. S., and Ahn, H. S., "Design and Implementation of a New Clamping Force Estimator in Electro-Mechanical Brake Systems," *International Journal of Automotive Technology*, Vol. 14, No. 5, pp. 739-745, Feb. 2013.

[33] 신동환, 권오석, 배준형, "웨지 구조를 이용한 전기기계브레이크 시스템 연구," 한국자동차공학회 논문집, 제 18 권, 제 3 호, pp. 8-18, 2010 년 5 월.

[34] Shin, D. H., Lee, S., et al., "Analytic Approaches for Keeping High Braking Efficiency and Clamping Efficiency of Electro Wedge Brakes," *International Journal of Precision Engineering and Manufacturing*, Vol. 16, No. 7, pp. 1609-1615, Jun. 2015.

[35] 한광진, 허건수, “Electro Wedge Brake 의 모델링 및 제어기 설계,” 한국자동차공학회 논문집, 제 20 권, 제 1 호, pp. 112-118, 2012 년 1 월.

[36] Hartmann, H., Schautt, M., Pascucci, A., and Gombert, B., “eBrake – the mechatronic wedge brake,” *SAE Tech. Paper 2002-01-2582*, 2001.

[37] Roberts, R., Schautt, M., Hartmann H., et al., “Modeling and validation of the mechatronic wedge brake,” *SAE Tech. Paper 2003-01-3331*, 2003.

[38] Fox, J., Roberts, R., Baier-Welt, C., Ho, L. M., Lacraru, L., Gombert, B., “Modeling and Control of a Single Motor Electronic Wedge Brake,” *SAE Tech. Paper 2007-01-0866*, 2006.

[39] 김민회, 정장식, 영구자석 동기 전동기 서보 시스템 제어와 실습, 보성각, 2006.

[40] Jeong, Y., Sul. S., Schulz, S., and Patel, N., “Fault Detection and Fault-Tolerant Control of Interior Permanent Magnet Motor Drive System for Electric Vehicle,” *IEEE Trans. on Industry Applications*, Vol. 41, No. 1, pp. 46-51, Jan. 2005.

[41] Park, G., Lee, S., Jin, S., and Kwak, S., “Integrated modeling and analysis of dynamics for electric vehicle powertrains,” *Expert Systems with Applications*, 41(5), pp. 2595-2607, Apr. 2014.

[42] Hwang, W., Han, K., Huh, K., Jung, J., and Kim, M., “Model-based Sensor Fault Detection Algorithm Design for Electro-Mechanical Brake,” *14th International IEEE Conference on Intelligent Transportation Systems*, Washington, DC, USA, Oct. 2011.

[43] Olsson, H., Å ström, K. J., Canudas de Wit, C., Gäfvert, M., and Lischinsky, P., “Friction models and friction compensation,” *European Journal of Control*, 4(3), pp. 176-195, 1998.

[44] 김상훈, 모터제어 – DC, AC, BLDC, 복두출판사, 2014.

[45] 설승기, 전기기기 제어론, 홍릉과학출판사, 2002.

[46] 이주, 김기찬, 안준선, 원성홍, 매입자석 동기모터의 설계 및 제어, 한양대학교 에너지변환연구실, 교보문고, 2010.

[47] Cesario, N., Taglialatela, F., and Lavorgna, M., “Adaptive Control Strategies for Electro-Mechanical Brakes,” *SAE Tech. Paper 2007-01-3944*, 2007.

[48] Anwar, S., *Fault Tolerant Drive By Wire Systems: Impact on Vehicle Safety and Reliability*, Bentham Science Publishers, 2012.

[49] Anwar, S., and Chen, L., “An Analytical Redundancy Based Fault Detection

and Isolation Algorithm for a Road-Wheel Control Subsystem in a Steer-By-Wire System," *IEEE Trans. on Vehicular Technology*, Vol. 56, No. 5, pp. 2859-2869, Sept. 2007.

[50] Higgins, A., and Koucky, S., "Mercedes pumps fly-by-wire brakes into new SL roadster," *Machine Design*, Vol. 74, No. 9, p. 26, May 2002.

[51] Isermann, R., Schwarz, R., and Stölzl, S., "Fault Tolerant Drive-By-Wire Systems," *IEEE Control Systems Magazine*, pp. 64-81, Oct. 2002.

[52] Assaleh, K., Shanableh, T., and Kheil, Y. A., "Group Method of Data Handling for Modeling Magnetorheological Dampers," *Intelligent Control and Automation*, Vol. 4, No. 1, pp. 70-79, 2013.

[53] López-Molina, T., Pérez-Méndez, A., and Rivas-Echeveria, F., "Data Analysis Techniques for Neural Networks-based Virtual Sensors," *in Proc. of the 8th WSEAS Int. Conf. on Neural Networks*, Vancouver, British Columbia, Canada, pp. 76-83, Jun. 2007.

[54] Baha, H., and Dibi, Z., "A Novel Neural Network-based Technique for Smart Gas Sensors Operating in a Dynamic Environment," *Sensors*, Vol. 9, No. 11, pp. 8944-8960, Nov. 2009.

[55] Ivakhnenko, A. G., "Polynomial Theory of Complex Systems," *IEEE Trans. on*

Systems, Man, and Cybernetics, Vol. SMC-1, No. 4, pp. 364-378, Oct. 1971.

[56] Lim, D. H., Lee, S. H., and Na, M. G., "Smart Soft-Sensing for the Feedwater Flowrate at PWRs Using a GMDH Algorithm," *IEEE Trans. on Nuclear Science*, Vol. 57, No. 1, pp. 340-347, Feb. 2010.

[57] Kim, J. H., Matsui, Y., Hayakawa, S., Suzuki, T., Okuma, S., and Tsuchida, N., "Acquisition and Modeling of Driving Skills by Using Three Dimensional Driving Simulator," *IEICE Trans. on Fundamentals of Electronics, Communications and Computer Sciences*, Vol. E88-A, No. 3, pp. 770-778, Mar. 2005.

[58] Mrugalski, M., Witczak, M., Korbicz, J., "Confidence Estimation of the Multi-Layer Perceptron and Its Application in Fault Detection Systems," *Engineering Applications of Artificial Intelligence*, 21(6), pp. 895-906, Sept. 2008.

[59] Chang, C., and Roschke, P., "Neural Network Modeling of a Magnetorheological Damper," *Journal of Intelligent Material Systems and Structures*, 9(9), pp. 755-764, Sept. 1998.

[60] Yager, R., and Filev, D., "Essentials of Fuzzy Modeling and Control," *SIGART Bulletin*, Vol. 6, No. 4, pp. 22-23, 1994.

[61] Korbicz, J., Metenidis, M. F., Mrugalski, M., and Witczak, M., "Confidence Estimation of GMDH Neural Networks," *Int. Conf. on Artificial Intelligence and*

Soft Computing, pp. 210-216, 2004.

[62] Korbicz, J., and Mrugalski, M., "Confidence Estimation of GMDH Neural Networks and Its Application in Fault Detection Systems," *International Journal of Systems Science*, 39(8), pp. 783-800, May 2008.

[63] Kondo, T., "GMDH Neural Network Algorithm Using the Heuristic Self-Organization Method and Its Application to the Pattern Identification Problem," *Proc. of the 37th SICE Annual Conference*, pp. 1143-1148, Jul. 1998.

[64] Kondo, T., Ueno, J., and Kondo, K., "Revised GMDH-Type Neural Networks Using AIC or PSS Criterion and Their Application to Medical Image Recognition," *Journal of Advanced Computational Intelligence and Intelligent Informatics*, 9(3), pp. 257-267, 2005.

[65] Kim, Y. W., Matsuda, R., Narikiyo, T., and Kim, J. H., "Attitude Control of Planar Space Robot Based on Self-Organizing Data Mining Algorithm," *Int. Conf. on Control, Automation and Systems (ICCAS)*, Gyeonggi-do, Korea, pp. 377-382, Jun. 2005.

[66] Iwasaki, M, Takei, H., and Matsui, N., "GMDH-based Modeling and Feedforward Compensation for Nonlinear Friction in Table Drive Systems," *IEEE Trans. on Industrial Electronics*, Vol. 50, No. 6, pp. 1172-1178, Dec. 2003.

[67] Nariman-Zadeh, N., Darvizeh, A., Jamali, A., and Moeini, A., "Evolutionary Design of Generalized Polynomial Neural Networks for Modeling and Prediction of Explosive Forming Process," *Journal of Material Processing and Technology*, Vol. 164-165, pp. 1516-1571, May 2005.

[68] Nariman-Zadeh, N., and Jamali, A., "Pareto Genetic Design of GMDH-Type Neural Networks for Nonlinear Systems," *Int. Workshop on Inductive Modeling*, Prague, Czech Republic, pp. 96-103, 2006.

[69] Hoseinnezhad, R., and Bab-Hadiashar, A., "Missing Data Compensation for Safety-Critical Components in a Drive-By-Wire System," *IEEE Trans. on Vehicular Technology*, Vol. 54, No. 4, pp. 1304-1311, Jul. 2005.

[70] Bae, J., Lee, S., Shin, D. H., Hong, J., Lee, J., and Kim, J. H., "Nonlinear Identification of Electronic Brake Pedal Behavior Using Hybrid GMDH and Genetic Algorithm in Brake-By-Wire System," *Journal of Electrical Engineering and Technology*, Vol. 12, No. 3, pp. 1292-1298, May 2017.

[71] Bae, J., Lee, S., Shin, D. H., Hong, J., Lee, J., and Kim, J. H., "A Soft Computing Approach for Brake Pedal Behavior Identification in Brake-By-Wire System," *16th Int. Conf. on Control, Automation and Systems (ICCAS)*, Gyeongju, Korea, pp. 1426-1429, Oct. 2016.

[72] www.ensatek.com.tr/image/urun/ec4pole/5EC-4POLE30_200.pdf.

[73] www.dewetron.co.kr/downloads.

[74] Choi, C., Lee, K., and Lee, W., "Observer-Based Phase Shift Fault Detection Using Adaptive Threshold for Rotor Position Sensor of Permanent Magnet Synchronous Machine Drives in Electromechanical Brake," *IEEE Trans. on Industrial Electronics*, Vol. 62, No. 3, pp. 1964-1974, Mar. 2015.

[75] Iizuk, K., Uzuhashi, H., Kano, M., Endo, T., and Mohri, K., "Microcomputer Control for Sensorless Brushless Motor," *IEEE Trans. on Industry Applications*, Vol. IA-21, No. 3, pp. 595-601, May 1985.

[76] Lee, K., and Lee, W., "A Study on Clamping Force Estimation of EMB for Fuel-Cell Vehicle Using Sliding Mode Observer," 28th *Int. Electric Vehicle Symposium and Exhibition (EVS28)*, Goyang, Korea, May 2015.

[77] Han, Y., Choi, J., and Kim, Y., "Sensorless PMSM Drive with a Sliding Mode Control Based Adaptive Speed and Stator Resistance Estimator," *IEEE Trans. on Magnetics*, Vol. 36, No. 5, pp. 3588-3591, Sept. 2000.

[78] Kim, H. W., and Sul, S. K., "A New Motor Speed Estimator Using Kalman Filter in Low-Speed Range," *IEEE Trans. on Industrial Electronics*, Vol. 43, No. 4, pp. 498-504, Aug. 1996.

[79] Qiu, A., and Wu, B., “Sensorless Control of Permanent Magnet Synchronous Motor Using Extended Kalman Filter,” *Canadian Conf. on Electrical and Computer Engineering (CCECE)*, pp. 1557-1562, May 2004.

[80] Warwick, K., Kang, Y. H., and Mitchell, R. J., “Genetic Least Squares for System Identification,” *Soft Computing*, 3(4), pp. 200-205, Dec. 1999.

[81] 박기서, 최세범, 현동윤, “전동식 브레이크 시스템의 클램핑력 센서 교정 및 클램핑력 추정 알고리즘 개발,” 한국자동차공학회 논문집, 제 24 권, 제 3 호, pp. 365-371, 2016 년 5 월.

[82] 정승환, 이형철, “Electronic Wedge Brake 시스템의 클램핑력 추정 및 Failsafe 제어 알고리즘 설계에 관한 연구,” 한국자동차공학회 논문집, 제 24 권, 제 1 호, pp. 16-23, 2016 년 1 월.

[83] Tamari, J., Doi, K., and Tamasho, T., “Prediction of Contact Pressure of Disc Brake Pad,” *JSAE Review*, 21(1), pp. 136-138, Jan. 2000.

[84] Kalman, R. E., “A New Approach to Linear Filtering and Prediction Problems,” *Trans. of the ASME – Journal of Basic Engineering*, 82(1), pp. 35-45, Mar. 1960.

[85] 배준형, 현유진, 이종훈, “$\alpha\beta$ 필터 및 NNPDA 알고리즘을 이용한

차량용 레이더 표적 추적 시스템 설계," 대한임베디드공학회 논문지, 제 6 권, 제 1 호, pp. 16-24, 2011 년 2 월.

[86] Faragher, R., "Understanding the Basis of the Kalman Filter Via a Simple and Intuitive Derivation," *IEEE Signal Processing Magazine*, Vol. 29, No. 5, pp. 128-132, Sept. 2012.

[87] Simon, D., *Optimal State Estimation: Kalman, H_∞, and Nonlinear Approaches*, John Wiley & Sons, 2006.

[88] Brown, R. G., and Hwang, P., *Introduction to Random Signals and Applied Kalman Filtering with MATLAB Exercises*, John Wiley & Sons, 4th Edition, 2012.

[89] Grewal, M. S., and Andrews, A. P., *Kalman Filtering: Theory and Practice with MATLAB*, John Wiley & Sons, 4th Edition, 2014.

[90] Holland, J. H., *Adaptation in Natural and Artificial Systems*, Ann Arbor, MI: University of Michigan, 1975.

[91] Shi, K. L., and Li, H., "Optimized PWM Strategy Based on Genetic Algorithms," *IEEE Trans. on Industrial Electronics*, Vol. 52, No. 5, pp. 1458-1461, Oct. 2005.

요 약 문

전기기계식 브레이크 기반 Brake-By-Wire 시스템에서의 센서리스 제어를 위한 소프트 컴퓨팅 접근법

본 논문에서는 전기기계식 브레이크 (EMB) 기반 brake-by-wire (BBW) 시스템에서의 센서리스 고장 허용 제어를 위한 새로운 소프트 컴퓨팅 기법을 제안한다.

현재 자동차 산업에서 BBW 시스템에 관한 연구가 활발히 진행되고 있다. 최근 하이브리드 자동차 및 전기 자동차에 브레이크 액츄에이터로 사용되는 EMB 를 장착하는 연구가 진행되고 있고, 이러한 EMB 시스템의 신뢰성을 위해서 전기 및 전자 시스템에 고장이 발생하여도 클램핑력 데이터가 손실되지 않아야 한다.

본 연구에서는 우선 EMB 시스템의 전동기와 기구부의 수학적 모델을 정립하였고, 캐스캐이드 형태의 PI 제어기가 EMB 모델을 기반으로 설계되었다. 기구부는 감속 기어, 스크류 나사 기어, 내/외부 패드 및 캘리퍼로 구성된다. 전동기에는 영구자석 동기 전동기 (PMSM)를 사용하였으며, 마이크로 컨트롤러와 인버터를 포함한 전자 제어 유닛 (ECU)을 구성하여 실험을 수행하였다. EMB 제어기는 캐스캐이드 PI 제어로 구성되며 클램핑력 제어기, 속도 제어기, 전류 제어기가 외부에서부터 내부의 순서로 배치된다. 캐스캐이드 PI 제어기의 이득은 전동기의 파라미터 값을 이용하여 매우 쉽게 조정할 수 있게 설계되었다. 또한 최적의 토크 운전을 보장하기 위해 벡터

제어 기법이 적용되었다.

본 논문의 목적은 신경망, 퍼지 및 유전자 알고리즘과 같은 소프트 컴퓨팅 기법을 이용하여 BBW 시스템의 전자식 브레이크 페달 센서 시스템과 클램핑력 센서에서 발생할 수 있는 고장에 대비하거나 센서리스 제어를 위한 하이브리드 형태의 새로운 시스템 식별과 추정 기법을 적용하는 것이다.

첫 번째로, group method of data handling (GMDH)과 유전자 알고리즘을 혼합한 하이브리드 식별 기법에 기반한 가상의 전자식 브레이크 페달 시스템을 제안한다. GMDH 의 주된 아이디어는 회귀 기법을 이용하여 계수를 얻은 2 차의 노드 전달 함수를 기반으로 피드포워드 네트워크에서 해석적 함수를 만드는 것이다. 해석적인 GMDH 모델이 성립되면 이 모델을 이용한 응용은 다른 식별 기법에 비해 매우 빠르고 계산량이 적다. 본 연구에서는 GMDH 의 최적의 네트워크 아키텍처를 산출하기 위해 유전자 알고리즘을 혼합하여 전체 아키텍처를 설계하는 새로운 접근 방식을 EMB 시스템에 적용하였다.

두 번째로, EMB 액츄에이터 부분에서 클램핑력의 추정에 관하여 연구하였다. EMB 제어 시스템에 사용되는 주요 센서로는 클램핑력을 측정하는 클램핑력 센서, 모터 회전각을 측정하는 위치 센서 및 3 상 모터의 전류를 측정하는 전류 센서이다. 각 센서의 고장을 판단하고 고장이 발생하였을 때 또는 비용과 구현 측면에서 센서없이 개발할 경우 실제 측정값을 추정값으로 대체할 필요성이 있다. 본 연구에서는 클램핑 및 릴리징 시 히스테리시스를 고려한 정확한 클램핑력 추정 기법을 제안하였다. 동적 강성 모델과 토크 평형 모델을 정립하고 유전자 알고리즘으로 최적화된 새로운 칼만 필터 알고리즘을

제시하여 두 모델을 결합하고 클램핑력을 추정하였다. 유전 알고리즘의 적용은 칼만 필터의 노이즈 공분산 행렬을 최적화하여 추정 정확도를 향상시키고, 고성능의 병렬 프로세서 사용 시 온라인 추정도 가능하게 한다.

마지막으로 실험을 통해 제안된 알고리즘들의 성능을 검증하였다.

핵심어: Brake-by-wire, 전기기계식 브레이크, Group method of data handling, 유전자 알고리즘, 칼만 필터